The FIRST Survey: Faint Images of the Radio Sky at Twenty-cm

Robert H. Becker
Department of Physics, University of California
Davis, CA 95616; and Institute of Geophysics and Planetary Physics,
Lawrence Livermore National Laboratory, Livermore, CA 94450

Richard L. White
Space Telescope Science Institute
3700 San Martin Drive, Baltimore, MD 21218

and

David J. Helfand
Department of Astronomy and Columbia Astrophysics Laboratory
538 West 120th Street, New York, NY 10027

Abstract

The *FIRST* survey to produce Faint Images of the Radio Sky at Twenty-cm is now underway using the NRAO Very Large Array. We describe here the scientific motivation for a large-area sky survey at radio frequencies which has a sensitivity and angular resolution comparable to the Palomar Observatory Sky Survey, and recount the history that led to the current survey project. The technical design of the survey is covered in detail, including a description and justification of the grid pattern chosen, the rationale behind the integration time and angular resolution selected, and a summary of the other considerations which informed our planning for the project. A comprehensive description of the automated data analysis pipeline we have developed is presented.

We also report here the results of the first year of *FIRST* observations. A total of 144 hours of time in April and May of 1993 were used for a variety of tests, as well as to cover an initial strip of the survey extending between $07^{\rm h}15^{\rm m}$ and $16^{\rm h}30^{\rm m}$ in a 2.8 degree-wide declination zone passing through the local zenith ($28.2 < \delta < 31.0$). A total of 2153 individual pointings yielded an image database containing 1039 merged images $46.5' \times 34.5'$ in extent with $1.8''$ pixels and a typical rms of 0.13 mJy. A catalog derived from this 300 deg^2 region contains 28,000 radio sources. We have performed extensive tests on the images and source list in order to establish the photometric and astrometric accuracy of these data products. We find systematic astrometric errors of $< 0.05''$; individual sources down to the 1 mJy survey flux density threshold have 90% confidence error circles with radii of $< 1''$. CLEAN bias introduces a systematic underestimate of point source flux densities of ~ 0.25 mJy; the bias is more severe for extended sources. Nonetheless, a comparison with a published deep survey field demonstrates that we successfully detect 39/49 sources with integrated flux densities > 0.75 mJy, including 19 of 20 sources above 2.0 mJy; the sources not detected are known to be very extended and so have surface brightnesses well below our threshold.

With the 480 hours of observing time committed for each of the next three B-configuration periods, *FIRST* will complete nearly one-half of its goal of covering the

10,000 deg^2 of the north Galactic cap scheduled for inclusion in the Sloan Digital Sky Survey. All of the *FIRST* data — raw visibilities, self-calibrated UV datasets, individual pointing maps, final merged images, source catalogs, and individual source images — are being placed in the public domain as soon as they are verified; all of the 1993 data are now available through the NRAO and/or the STScI archive. We conclude with a brief summary of the scientific significance of *FIRST*, which represents an improvement by a factor of 50 in both angular resolution and sensitivity over the best available large area radio surveys.

1. Introduction

In April 1943, the "amateur" radio astronomer Grote Reber began the first systematic survey of the radio Universe. Using a backyard telescope with a beamwidth of 16 degrees operating at a frequency of 150 MHz, he spent most of the following year mapping the northern sky to a flux density threshold of a few thousand Janskys. The results, published in the *Astrophysical Journal* in the form of strip chart recorder reproductions (Reber 1944), revealed several areas of enhanced emission lying along the plane of the Milky Way, demonstrated that the emission centroid lay 30 degrees from the then-used zero point of Galactic longitude, and provided the first image of the Universe outside the traditional optical window.

Fifty years later, in April of last year, we began our first *FIRST* survey at radio wavelengths. To produce *Faint Images of the Radio Sky at Twenty-cm* will take approximately the same amount of time as Reber's work, but the final map will have 10^8 more resolution elements and will reach a sensitivity five million times greater. Using the NRAO[1] Very Large Array (VLA) in its B-configuration, we will cover 10,000 $\deg^2$ of the northern Galactic cap to a flux density limit of 1.0 mJy with an angular resolution of better than $5''$. The principal data products will be (1) a sky map containing 4×10^{10} pixels with an rms noise of < 0.15 mJy, and (2) a 20 cm source catalog with flux densities, subarcsecond positions, and morphological information on over one million sources — in short, the radio equivalent of the *Palomar Sky Survey* for 25% of the celestial sphere.

We describe in this paper the motivation for a radio survey with this sensitivity and resolution, and place it in the context of other current and planned survey projects. We briefly outline the history of the *FIRST* project, from our original proposal in August of 1990 through the first round of observations in May of 1993. We describe in detail the survey design and present a comprehensive description of the data reduction and analysis system we have built and tested for generating the survey maps and catalogs. We demonstrate the realization of the *FIRST* survey's goals through the presentation of the 1039 coadded maps we have created from the 1993 data, and the numerous tests we have conducted to evaluate their astrometric, photometric, and morphological accuracy. A brief description of the radio source list we are extracting from the images is provided, although the catalog itself will be published separately. In the penultimate section, we present a precis of the numerous scientific problems which the *FIRST* survey will address. We conclude with our plan for distributing the fruits of the survey to the astronomical community.

2. Motivation

2.1. *Astronomical Sky Surveys*

Astronomy is an observational, rather than an experimental, science, and its practitioners carry out the equivalent of experiments by discovering, and then studying, astrophysical systems with a variety of ages and initial conditions. Surveys generate the list of available laboratories for such studies, and, as such, are central to progress in the discipline.

[1] The National Radio Astronomy Observatory is operated by Associated Universities, Inc., under cooperative agreement with the National Science Foundation.

Complete, unbiased surveys are the best technique we have *both* for discovering new and unexpected phenomena (Harwit 1981; Kellermann and Sheets 1983), *and* for deriving the intrinsic properties of source classes so that their underlying physics can be deduced. Recognizing this, optical astronomers began the first modern effort at a complete unbiased survey in 1949. The National Geographic-Palomar Observatory Sky Survey (POSS I) provides data on optical emitters over the entire northern sky in two colors down to a flux density limit of ~ 0.1 mJy and with arcsecond positional accuracy; it has been a fundamental resource ever since its creation, and the impending release of digital images and source catalogs based on this survey will only serve to enhance its importance to the discipline.

The radiation emitted by most astronomical objects is not, however, restricted to narrow ranges in the electromagnetic spectrum defined by atmospheric transparency or instrumental sensitivity limits. Thus, surveys in widely separated wavelength bands are essential in constructing accurate and complete pictures of various source populations. As each new window in the spectrum has opened over the past 30 years, major space missions have had as their first priority unbiased sky surveys: from SAS-2 to the Compton *GRO* in the gamma ray regime, *UHURU* to *ROSAT* in X-rays, and *IRAS* in the infrared, the source catalogs and sky maps produced by survey missions form a core resource for all of modern astrophysical research. With recent improvements in computing speed, storage capacity, database systems, and networks, the availability and utility of this resource is further enhanced. Projects currently being planned to carry out new ground-based surveys in the optical (the Sloan Digital Sky Survey, Gunn and Knapp 1992) and the near-infrared (the 2-micron Survey, Kleinmann 1992) will have equally major impacts on the field.

Radio astronomers have produced a large number of surveys over the fifty-year history of the discipline although, in the last three decades, their approach has often been to build special purpose telescopes for this task, while using the "premier" instruments of the day for detailed studies of individual objects and source classes. The series of Cambridge survey arrays, the Mills Cross and its successors, and the Texas 80-cm array are examples of special purpose instruments which have made major contributions to mapping the radio sky; the Texas survey catalog is the largest radio source list in existence with 80,000 entries (Douglas, private communication), although it has never been formally published. In the late 80's, the Green Bank 300-foot telescope, considered by some (prescient) astronomers to be in its dotage, was used by Condon and his collaborators to conduct perhaps the most widely used radio sky surveys at 6 cm and 20 cm (Condon and Broderick 1985, 1986; Condon Broderick and Seielstad 1989). Catalogs derived from the higher frequency survey have been produced by Becker, White, and Edwards (1991) and by Gregory and Condon (1991), and contain $\sim 53,500$ sources at 6cm down to a flux density threshold of ~ 30 mJy with $50''$ positions; White and Becker (1992) produced the analogous catalog at 20 cm which includes 30,329 sources with $160''$ positions and a limiting flux density of 100 mJy. Finally, a southern complement to the Green Bank surveys has recently been completed with the Parkes telescope (Wright et al. 1994); it has a flux density limit of 30 mJy at 6cm and positions good to $\sim 50''$. The maps and catalogs from this work represent the state of our knowledge of the radio sky at centimeter wavelengths.

These surveys do not, however, represent the best that is possible with today's radio telescopes. Pencil beam surveys made with the interferometric arrays at Westerbork and the VLA have reached flux densities a factor of 10^3 lower (Donnelly, Partridge, and Windhorst 1987; Windhorst et al. 1985; Mitchell and Condon 1985), revealing new populations of radio sources below a few mJy (e.g., Benn et al. 1993 and references therein). In addition, the hundred-fold improvement in angular resolution made possible with these instruments has shown that $\sim 70\%$ of the sources in single-dish catalogs (S > 30 mJy) are resolved on scales of $\sim 2''$ (Windhorst, Mathis, and Neuschaefer 1990). More importantly, since optical counterparts to centimetric sources are typically faint — $\sim 85\%$ of sources at 3 mJy have counterparts fainter than $m_v \sim 20$ (§3.1) — optical quality positions are required for determining source distances and studying their evolution. Until a few years ago, computing capacity was simply insufficient to contemplate a major sky survey using these instruments. This is no longer the case. Thus, both Westerbork and the VLA are now engaged in large-scale sky surveys. *FIRST* is the most sensitive of these.

FIRST represents a factor of ~ 50 improvement in limiting sensitivity over the best available sky survey at any radio wavelength. This is equivalent to the improvement in limiting magnitude that the Sloan Digital Sky Survey will achieve over the POSS I plates. In addition, it is a fully digital survey whose maps and catalogs will be instantly accessible to the astronomical community. More importantly, however, *FIRST* also represents a factor of 50 improvement in angular resolution and concomitant positional accuracy. As we show below, even the weakest sources will be located to $\lesssim 1''$. As a consequence, 15% of all detected objects will be immediately identifiable on the POSS I survey, and over 50% will have optical counterparts at the SDSS limit with a low chance coincidence rate. The final catalog will contain approximately one million radio sources.

2.2. *History*

On August 8, 1990, we submitted a proposal to the NRAO which began: "We propose to produce a centimeter-wave counterpart to the Palomar Observatory Sky Survey by using the VLA to map the northern sky." Our stated goals were a flux density limit of ~ 1 mJy and positional accuracies of $\lesssim 3''$. The timing of this proposal was a consequence of several factors. We were in the process of completing a multiwavelength survey of the Galactic plane at 6 cm, 20 cm, and 90 cm, and had worked through some of the problems attendant on producing and analyzing thousands of VLA images (Zoonematkermani et al. 1991; Becker et al. 1991; Helfand et al. 1993, and Becker et al. 1994); in addition, our generation of source catalogs from the Green Bank 6 cm and 20 cm surveys of Condon and Broderick (1986) and Condon et al. (1989) provided experience in the automated production of survey source lists. More importantly, the VLA was in the process of installing a new generation of 20 cm receivers which would lead to a sensitivity improvement of a full factor of two for all observations at this frequency. Also critical to the implementation of such a large-scale project was the rapid advance in workstation computing and storage capacity which generated affordable options for reducing the terabyte datasets involved in a high-resolution all-sky survey.

Our original proposal called for a survey covering the whole sky visible from the VLA ($-30 < \delta < +90$) using either the C-configuration, or, preferably, a specially designed hybrid configuration between B and C which would provide the resolution and positional accuracy of the B-configuration (a synthesized beam of $\sim 5''$), while retaining 6 of the antennas in their more compact, C-configuration positions in order to enhance our sensitivity to low surface brightness objects and sources extended on scales $> 30''$. The plan required a total of 123,750 1.5-minute snapshot observations in bandwidth synthesis mode to achieve a typical map rms of 0.20 mJy at field center; the projected source catalog would contain in excess of one million radio sources with positions accurate to $< 3''$. We proposed carrying out the survey by including one extra month that would be exclusively devoted to the survey in each of the six VLA configuration cycles following completion of the 20cm receiver upgrade; this would have allowed for completion of the survey by the end of the decade with minimal disruption to the rest of the VLA science program.

Following consultation with senior NRAO staff members, the Director informed us of his decision not to have the proposal refereed. During the ensuing eight months, we engaged in extensive discussions with the NRAO and with members of the community, and redesigned our proposal to meet some of the objections raised following the original submission. We adopted the standard C-configuration as the baseline array (with CnB for southern declination fields). As in our original proposal, we committed to releasing the final maps and catalogs within two years of each observing run (to allow for reobservation of problem fields); to demonstrate our ability to reduce and distribute the data in a timely manner, we proposed a ten-day pilot survey for the 1992 C-configuration cycle which we promised to deliver to the community within six months. In our cover letter for the resubmission of our proposal on 9 May 1991, we pointed out that during the period 1988–1990, 3% of all allocated VLA time was used for 20 cm snapshot observations; in that our survey would obviate the need for the vast majority of these observations, it would actually *increase* the amount of telescope time available for other science projects in the next decade.

Two weeks prior to this resubmission, the NRAO received another proposal from an internal team led by Dr. J. Condon to survey the sky north of $\delta = -30^\circ$ using the VLA at 20 cm. This proposal suggested a larger number of shorter pointings (190,000 30-second snapshots vs. 120,000 90-second snapshots). The most important difference, however, was that it proposed to use the D-configuration ($\sim 50''$ synthesized beam). The advantages cited for the lower-resolution survey were increased surface brightness sensitivity and simplification of the computational requirements, since the use of bandwidth synthesis mode would not be required to achieve the requisite wide-field mapping, and the maps would contain nine times fewer pixels owing to the larger beam size. The costs of going to the D configuration were an increased survey flux density threshold (~ 1.5 mJy vs. $\lesssim 1$ mJy),[2] lower accuracy positions, and decreased resolution for exploring source structure. The wider usable bandwidth in this array decreased the total survey time required by a factor of two (albeit, at the loss of a factor of 1.5 in threshold sensitivity). In addition, all observations need to be conducted at night in order to minimize man-made interference to which the D configuration is more susceptible. Furthermore, using a small number of broad frequency channels places strong limitations on one's ability to excise narrow-band interference.

Both proposals were refereed in the summer of 1991. There was widespread support among the referees for a VLA sky survey, but no consensus as to which survey should be done. During the 1992 C and D configurations, a 25 deg^2 region was surveyed twice

[2] The *NVSS* is actually achieving a flux density limit of 2.5 mJy.

with the respective survey parameters in order to provide some empirical data with which to make a judgement concerning the relative merits of the two approaches. In November 1992, a special panel including NRAO and non-NRAO scientists was convened to hear presentations from both survey teams. Their recommendation, accepted by the Director, was that two surveys be done. The D-configuration survey, now known as the NRAO VLA Sky Survey *(NVSS)*, was extended to cover the entire sky north of $\delta = -40°$ and was scheduled to be completed over the next three configuration cycles. In addition, convinced of the desirability of accurate source positions for optical followup, the virtue of a deeper survey unaffected by source confusion, and the importance of high angular resolution for morphological studies, the committee recommended that our team conduct a survey using the B-configuration (synthesized beam $\sim 5''$) that would cover a region of the north Galactic cap scheduled for observation with the Sloan Digital Sky Survey. Both teams accepted this charge. The high-resolution survey team chose *FIRST* as its moniker.

An enlarged and reconstituted Survey Oversight Committee met in March of 1993 to review this decision and to begin their task of monitoring its detailed implementation. A common pointing grid designed by one of us (RLW) was adopted for both surveys and is described in detail below (§4.1). The integration time per field was set at 165 seconds for the B-configuration survey in order to achieve a submilliJansky point source threshold. The first *FIRST* observations were scheduled in April 1993, with a total of 144 hours completed by the end of the B-configuration in May. Apart from a few isolated observations designed to overlap existing deep survey fields and to test the daytime interference environment, coverage included a contiguous strip $\sim$ 2.8 degrees wide near the local zenith (see §5). Recently completed observations during the 1994 season extend this strip by 10 degrees in declination, and bring the total area covered to 1600 deg^2.

2.3. *Non-proprietary Data Policy*

As we had originally proposed, the standard VLA proprietary period of eighteen months is waived for all *FIRST* data; i.e., the raw UV data are available from the VLA archive the day they are taken. In addition, we have agreed to provide fully self-calibrated UV datasets for each observation to the NRAO for distribution to any interested users; all data taken in 1993 and 1994 are now available. More importantly, we are creating a public archive of all survey images and catalogs as soon as they are fully tested for quality and accuracy. This includes the individual CLEANed maps from each pointing as well as the coadded images (see below) which form the principal survey product. In addition, an annotated source catalog and individual "postage stamp" images of each source are being made available. Information on retrieving any of these data products can be obtained from the *FIRST* home page on World Wide Web (http://sundog.stsci.edu/). Images and a source catalog from the 1993 observations are now available.

3. Scientific Priorities for the Survey

The primary desiderata for the design of the *FIRST* survey were:

- positional accuracy sufficient to achieve a large number of optical identifications with low chance coincidence rates;
- sensitivity sufficient to probe populations below the break in the radio $\log N - \log S$ curve;

- angular resolution sufficient to provide for morphological classification of sources and avoidance of source confusion in regions such as high redshift galaxy clusters which have an angular scale of $\sim 1'$.

We discuss each of these issues briefly here.

3.1. *Source Positions*

While considerable information on the source type and radiation mechanism of a radio emitter can be derived from observations of its radio morphology, spectrum, and polarization characteristics, optical observations are still required to establish the source's distance and to classify it unambiguously. Given the faint magnitudes of optical counterparts to radio sources at the mJy level — a $\sim 50\%$ identification rate is only achieved at $m_v \sim 24.0$ (Kron, Koo, and Windhorst 1985) — and the high surface density of optical objects on the sky at these magnitudes ($> 10^4$ deg^{-2}), accurate radio positions are required to obtain high reliability identifications with a low rate of chance coincidences. FIGURE 1 displays the false identification rate as a function of optical source density which led to the choice of the B-configuration for the *FIRST* survey. At the POSS I limit of $m_v \sim 20$, 50% of the sky has a surface density in stars and galaxies of > 5000 deg^{-2}, producing a 25% false rate for the D-configuration survey. At the SDSS limit of $m_v \sim 24$, the entire *FIRST* survey region has a density $> 2.5 \times 10^4$ objects deg^{-2}, and the maximum surface density encountered is $> 5 \times 10^4$. This leads to a C-configuration false rate of $\sim 20\%$ and a D-configuration false rate of $> 60\%$, but leaves the B-configuration rate at less than 8%. In addition, the fact that 55% of sources which will appear point-like in the D-configuration are, in fact, extended and/or multiple sources (see §7.3) leads to an additional uncertainty in their positions and increased difficulty in finding optical counterparts. In §7.1, we show that we have achieved the theoretical positional accuracy of $\lesssim 1''$ using the B-configuration. In a subsequent paper, we demonstrate the practical implementation of an optical identification program for *FIRST* using the Cambridge/Institute of Astronomy APM scans of the POSS I plates (McMahon et al. 1995).

3.2. *Flux Density Limit*

FIGURE 2A presents the $\log N - \log S$ curve for radio sources observed at 20 cm (Condon 1984). At flux densities $\gtrsim 3$ mJy, the radio population is dominated by active galactic nuclei (AGN) including radio galaxies, BL Lac objects, and radio-loud quasars. Below 3 mJy, however, the $\log N - \log S$ curve flattens substantially, indicating the presence of a new population. Several authors (Windhorst et al. 1985; Oort 1987; and Thuan and Condon 1987) have identified this new component with moderate redshift star-forming galaxies. In FIGURE 2B, we show the expected contributions of these two principal source classes as a function of limiting flux density (Condon 1984). At the *FIRST* threshold, we will detect $\sim 750,000$ AGN and over 250,000 star-forming galaxies. §9 lists some of the scientific advances we can expect with such massive samples in hand.

3.3. *Source Morphology*

Radio sources exhibit a wide range of morphological types which provide clues to the source class, emission mechanism, and properties of the surrounding medium. Among high Galactic latitude sources, stars, radio pulsars, and many AGN such as BL Lac objects, OVV

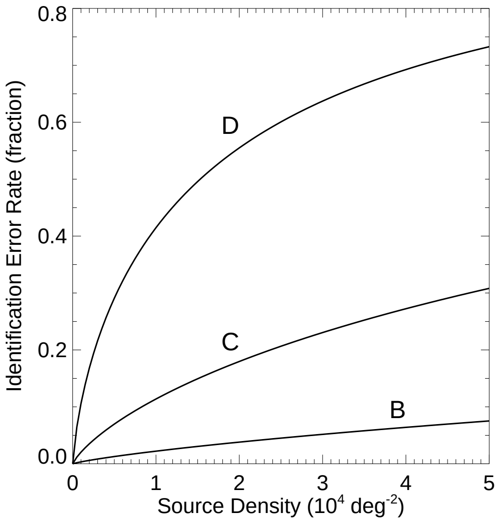

FIGURE 1(A)

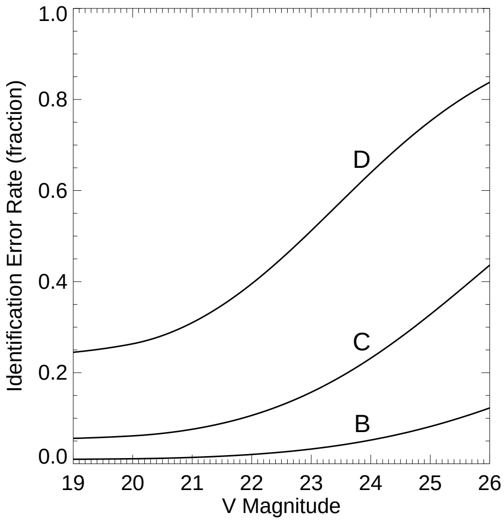

FIGURE 1(B)

FIGURE 1. (a) The radio source identification error rate as a function of density of candidates on the sky for 1.4 GHz VLA observations. The RMS position error for a radio source is taken as 1/10 FWHM beamwidth, appropriate for sources near the survey limit ($0.6''$, $1.8''$, and $5.4''$ for B, C, and D configurations respectively.) A matching radius was chosen such that the number of false IDs within the error circle is equal to number of true IDs missed due to errors in radio position. We assume that 30% of radio sources have true counterparts. (b) The identification error rate at the Galactic pole as function of optical brightness. Star densities are taken from Bahcall & Soneira (1980); galaxy densities are from Koo & Kron (1992). The fraction of radio sources with true optical counterparts is taken from Kron et al. (1985). The error rate does not improve much for $V < 21$ because the fraction of radio sources with optical counterparts declines about as rapidly as the optical source density.

quasars, and, in general, flat and inverted spectrum sources, are point-like at a resolution of a few arcseconds. Other AGN, from nearby low-power radio galaxies to distant quasars, display jets, halos, and large-scale radio lobes. When these objects are found in dense cluster environments, the lobes are often distorted by the motion of the parent galaxy through the intracluster medium, producing head-tail sources (Owen et al. 1979). Distant sources may be distorted into arcs of emission by gravitational focusing from foreground clusters (Soucail 1991). The thermal emission detected from star-forming galaxies may be highly concentrated in a nuclear starburst, or spread more generally throughout the galactic disk. Finally, the physical clustering of sources in galaxy groups, clusters, and larger scale structures can present a source confusion problem more severe than that determined from consideration of the $\log N - \log S$ alone. For the final adopted parameters of the *FIRST* survey, we reach a source surface density of ~ 100 sources deg^{-2} with 4×10^5 resolution elements deg^{-2}, a factor of 100 removed from the confusion limit.

The high angular resolution which allows detailed morphological studies, our optical-quality astrometry, and *FIRST*'s faint flux density threshold has a concomitant price: some of the flux from extended sources will be resolved out, leading to 1) a survey threshold that is a function of source size, and 2) the systematic underestimate of extended source

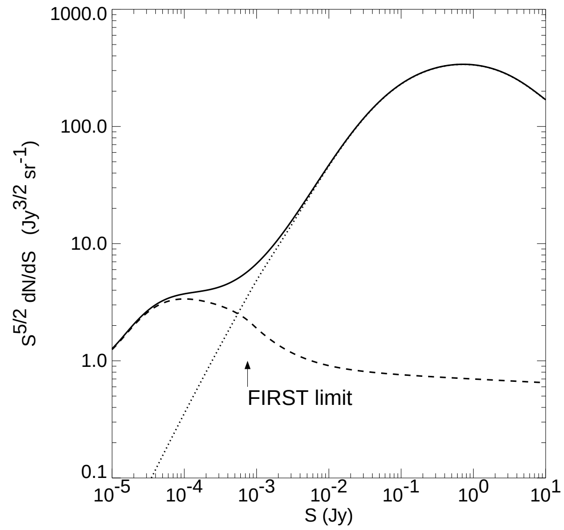

FIGURE 2(A)

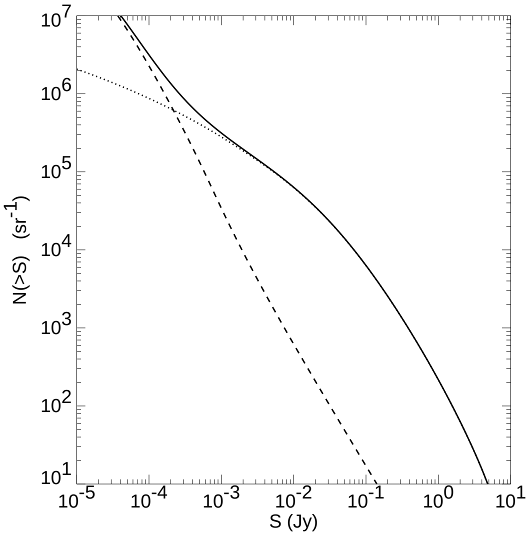

FIGURE 2(B)

FIGURE 2. (a) Source number density, dN/dS, versus flux density S at 20 cm (Condon 1984, Windhorst 1985). Short and long dashes represent the contributions from AGN and star forming galaxies, respectively. (b) The relative contributions of star forming galaxies and AGN to the cumulative radio source counts as a function of 20 cm flux density.

flux densities. The magnitude of these effects depends on the intrinsic size distribution for the sources of interest. Windhorst et al. (1990) have examined the size distribution of faint radio sources by collecting data from all of the major 1.4 GHz surveys, and deriving expressions for the mean angular size as a function of flux density, as well as the integral angular size distribution function. They find

$$h(\psi) = \exp\left[-(\ln 2)(\psi/\psi_{\rm med})^{0.62}\right], \tag{1}$$

where $h(\psi)$ is the fraction of sources larger than angular size ψ, and the median angular size $\psi_{\rm med}$ at flux density S is given by

$$\psi_{\rm med} = 2.0 S^{0.30} \text{ arcsec}, \tag{2}$$

where S is measured in mJy at 1.4 GHz.

As shown in §7, the fraction of the flux density from a Gaussian source resolved out by the B configuration is only 3% at 18″ FWHM, 16% at 24″, and 23% at 30″. However, CLEAN bias (also discussed in §7) is a larger problem for extended sources, and must be included in a calculation of the fraction of sources that will be missing from any *FIRST* catalog as a result of resolution effects. In TABLE 1, we tabulate the values of $\psi_{\rm med}$, $\psi_{\rm crit}$, and $[1 - h(\psi_{\rm crit})]$ for flux density levels ranging from 30 mJy (the limit of the best existing centimetric catalog) to 1 mJy; $\psi_{\rm crit}$ is the angular size at which, owing to CLEAN bias and resolution effects, a source falls below our search algorithm's peak flux density threshold of 0.75 mJy.

These estimates suggest we will miss $\sim 15\%$ of sources with integrated flux densities between 5 and 50 mJy, and one third of all sources between 1 and 5 mJy. However, this estimate is too pessimistic for several reasons. First, using a peak-flux search algorithm to find extended sources on maps optimized for point source sensitivity (e.g., made using natural weighting) is far from the optimal strategy for finding extended objects; indeed, as we show in §7.2, a much larger fraction of faint sources actually appear in our maps. Secondly, the numbers in the table have been calculated from experiments which insert Gaussian sources of various sizes into our raw UV data and then determine what fraction of the true flux density is recovered in the maps. Real extended objects, however, often have bright, compact features which will raise the peak flux density in the map above our threshold.

The VLA A-configuration observations of the Westerbork Leiden-Berkeley Deep Survey sources (Oort et al. 1987; Oort 1988) demonstrate this latter effect. A total of 145 sources with integrated flux densities > 0.75 mJy at 20 cm (as detected with the $12''$ Westerbork beam) were observed at the VLA; 14 of the larger objects were resolved into multiple components. After accounting for CLEAN bias and resolution effects, and imposing a 0.75 mJy peak flux density threshold, we would detect all but 20 of the 166 components. We would miss $\sim 30\%$ of those between 1 and 2 mJy, $\sim 5\%$ of sources from 2 to 5 mJy, and only 1 of the 82 sources brighter than 5 mJy. This is consistent with the comparison of our images with a VLA deep survey of the same region which we present in §7.2.

4. Technical Design of the Survey

The scientific issues and historical developments outlined above led us to design the *FIRST* survey with the following specific goals:

(i) flux density limit ~ 1 mJy;
(ii) astrometric accuracy for the faintest sources of $< 1''$; and
(iii) sky coverage matching the SDSS survey region of the north Galactic cap.

In addition, uniformity of sensitivity over the full survey area and maximum achievable observing efficiency were important considerations, as were our ability to reduce and analyze the data in a timely fashion. We present here our solutions to the problems of sky coverage, efficiency and uniformity as well as other technical considerations involved in planning the survey, while the following section describes in detail how the observations are actually undertaken.

4.1. *The Coverage Grid*

The goal of the survey is to produce a continuous, uniform-sensitivity 1.4 GHz image covering the north Galactic cap. The grid of pointing positions is chosen so that when the individual field maps are coadded (see §6) the resulting images have nearly the same sensitivity at field centers as at the "seams" between the fields. As discussed by Condon et al. (1994), the optimal grid would be a simple hexagonal pattern if the sky were flat, but is more complicated on the celestial sphere. We designed the grid for the *FIRST* survey based on several requirements:

(1) The B-configuration survey and the D-configuration (*NVSS*) survey must share the same grid so that it is possible to combine the data from the two configurations.
(2) The grid pointing centers must lie along lines of constant right ascension and declination for efficient observation by the VLA.
(3) The integration plus slew time for each field must be a multiple of 10 seconds. This precludes solutions that vary the integration time to achieve uniform sensitivity.
(4) The grid must be efficient, reaching the best possible sensitivity with a minimum of observing time.

J. Condon originally proposed dividing the sky into declination strips with each strip having a fixed RA and Dec spacing. This pattern is inefficient for two reasons. First, since lines of constant RA converge as they move away from the equator, the pointing centers are more closely packed at the high-declination edge of each strip than at the low-declination edge. To avoid wide variations in sensitivity it is therefore necessary for the declination strips to be relatively narrow ($\sim 8°$–$10°$), and even these strips waste some observing time near the high-declination edge because the centers are too closely spaced. Second, it is necessary to observe the declination line at the boundaries between strips twice (with two different RA spacings) to avoid low-sensitivity holes in the coadded maps near the boundary. This makes narrow strips inefficient.

The solution to these problems is to keep the RA spacing fixed within strips but to allow the declination spacing to vary. At higher declinations, where the constant RA lines have converged, the declination spacing is correspondingly increased so that the sensitivity in the coadded map remains constant. The declination spacing required is roughly $\Delta\delta \propto 1/\cos\delta$, which leads to a constant number of pointing centers per unit area on the sphere; the actual spacing we are using was computed so that the worst-case sensitivity at any point in the coadded maps is the same everywhere in the sky.

With variable declination spacing, the declination strips can be much wider while still retaining high efficiency. A regular hexagonal grid can be oriented along lines of RA and declination in two different ways (see Fig. 3). If the distance between neighboring field centers is Δ, then the spacing along RA and declination lines is $\sqrt{3}\Delta$ in one direction and Δ in the other. A natural way to lay out the declination strips is to start with the grid oriented as in the lower panel of Figure 3 at the low-declination edge and to allow the squeezing in RA and stretching in declination to effect a gradual transformation of the grid to the upper orientation in Figure 3. This allows declination strips with $\cos\delta_{lo}/\cos\delta_{hi} = \sqrt{3}$; for example, a single declination strip can extend from 0° to 54.7°.

This scheme can be made even more efficient if we allow the declination strips to be slightly wider, so that $\cos\delta_{lo}/\cos\delta_{hi} = 2$. Then the RA spacing (which jumps at strip boundaries) changes by exactly a factor of 2 between strips. As a result, there is no need for duplicate observations along the boundary declination; instead, as one moves across the boundary, a seamless join between the two strips is achieved by dropping every other RA point (or two of every three points at the polar zone boundary) (Fig. 4). The resulting grid can be extended all the way to the celestial pole with 7 declination strips.

The actual RA and declination values for the grid are described in Tables 2 and 3. The grid covers the sky over the declination range −42° to +90°. The positions lie on lines of constant Right Ascension and Declination in J2000 coordinates. Within each of the

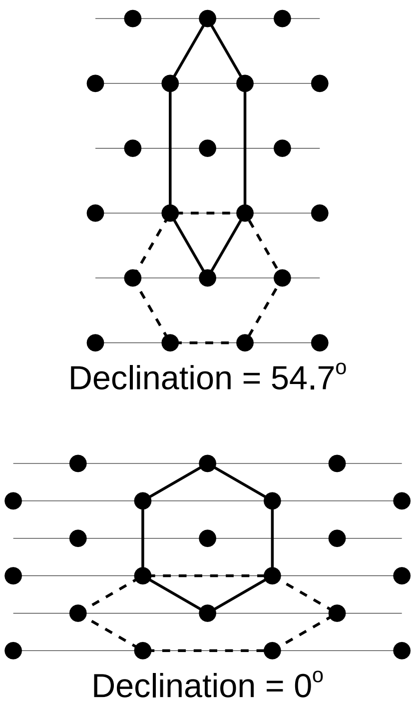

FIGURE 3. Two different ways a hexagonal grid can be oriented along RA and Dec lines. In the grid used for the survey, the hexagonal grid of pointing centers is gradually deformed from the bottom pattern to the top pattern as lines of constant RA squeeze together while lines of constant declination spread apart. This allows a seamless pointing grid from -60° to 60° declination while maintaining constant sensitivity.

seven distinct declination zones the number of RA points, NRA, is the same. A summary of the Dec zones is given in TABLE 2.

TABLE 3 gives the positions of the northern part of the survey grid. The pointing centers on adjacent declination lines are staggered in RA. For example, the Dec $= 0^\circ 0'$ line has RA $= 0^{\rm h}0^{\rm m}$, $0^{\rm h}3^{\rm m}$, etc., while the next line at Dec $= 0^\circ 13'$ has RA $= 0^{\rm h}1.5^{\rm m}$, $0^{\rm h}4.5^{\rm m}$, and so on. The RA values for row N are $\alpha_n = (n + E/2) \times \Delta\alpha$, $n = 0, 1, ..., NRA - 1$, where $E = 0$ if N is even and 1 if N is odd and $\Delta\alpha = 1440/NRA$ minutes.

The rows are numbered such that row 0 is at the pole. The grid is symmetrical about the equator, with row 356 on the equator, so the declination of row $356 + k$ is equal to minus the declination of row $356 - k$. This symmetry makes it simple to extend the grid farther south if desired. The number of fields covering the entire sky would be 265,452. For comparison, a “perfect” hexagonal grid with 26 arcmin spacing covering a plane area of 41,253 square degrees would require 253,677 pointings, so the average efficiency of this grid over the sky is 95.6%.

All declinations have been chosen to be integral multiples of 6 arcsec, and all RAs are integral multiples of 1.5 minutes of time. The positions can be specified exactly by giving the declination to an accuracy of 0.1 arcmin and the RA to 0.1 minute, allowing them to be coded in 11 characters: *hhmmm+ddmmm*.

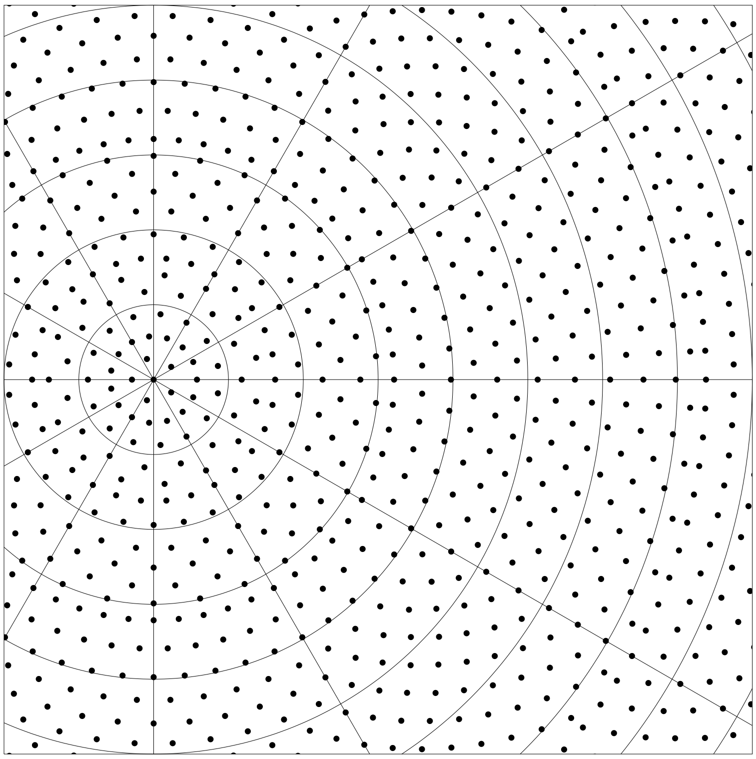

FIGURE 4. A region of the grid near the north celestial pole. The declination circles are at 1° intervals. There are boundaries between declination strips on circles of radius 0.3, 1.4, 3.0, and 7.3 degrees about the pole. The relatively smooth distribution of points indicates that the grid is efficient even near the pole. Far from the pole the efficiency is even better.

4.2. *Efficiency*

As discussed above, the optimization of the grid pattern was an essential step in making efficient use of the VLA. Another measure of efficiency is the fraction of observing time actually utilized in collecting survey data. There are two primary sources of overhead in carrying out the observations: slewing and calibration. The stability of the VLA at 20cm allows calibration to be held to a minimum. In general, calibrators are observed once an hour for 60 s. Furthermore, calibration sources which lie close to the grid locations are selected in order to minimize slew time. Typically, less than 2 minutes per hour, or 3% of the observing time, is employed in calibration. As for time spent slewing between grid points, the VLA staff developed a special mode for observing equally spaced fields situated along lines of constant RA or declination. Using this survey mode, slew times between adjacent fields average 10 s, and account for a total of 6% of the allocated observing time. Another 3% of the time is lost to VLA down-time and periods of extreme interference. In summary, then, the *FIRST* survey uses 88% of its allocated hours integrating on target, a measure of efficiency which exceeds that of most normal observing programs at the Observatory despite our short integration time on each survey field.

4.3. *Computing Tractability*

The reduction of the accumulated data is computer intensive and was a major concern in evaluating the viability of the *FIRST* survey. We have subsequently demonstrated that the timely reduction and analysis of the observations is a tractable problem. We have divided the computations into three modules, each of which is accomplished through the use of an AIPS script of our design—one for editing and self-calibration, one for imaging and CLEANing, and one for coadding. Using a SPARC 10/40 processor, the scripts require 0.5, 1.5, and 0.5 hours, respectively, of real time per image processed. We currently have four such processors, adequate for reducing all the data taken in a given B configuration before the beginning of the subsequent observing season. Details of the pipeline processing system are contained in §6.

4.4. *Other Considerations*

In order to map the full primary beam of the VLA antennas ($\sim 30'$) in the B configuration, it is essential to perform the observations in the bandwidth synthesis mode in order to avoid substantial bandwidth smearing. This requirement has ancillary consequences. A major advantage is interference suppression. Since narrow-band, man-made signals dominate the interference environment most of the time, judicious selection of the center frequency of each IF plus the editing of data on a channel by channel basis allows us to operate at any time of day with a very small amount of time lost to interference; in the 1993 data, fewer than 40 out of 2153 fields will require reobservation owing to interference of any type. Our selected channel width of 3 MHz leads to a limit on the reduction in peak intensity due to bandwidth smearing of $< 3\%$ at all points in the final coadded images.

The primary disadvantage to the bandwidth synthesis mode is the loss of half the available bandwidth owing to correlator limitations, and the concomitant loss of polarization information. Since the *NVSS* will achieve polarimetric measurements for all sources brighter than ~ 30 mJy (for a fractional polarization of 5%), and fainter sources will nearly all have unmeasurably low polarized signals, this is not a significant loss to the whole VLA sky survey program.

5. The Observations

Consistent with the above considerations, *FIRST* comprises a series of bandwidth synthesis snapshot observations using the 20 cm system in the B configuration of the VLA. The data are collected in spectral line mode using 2 (IFs) $\times 2$ (polarizations) $\times 7$ (frequency) channels, each 3 MHz wide and centered at 1365 and 1435 MHz; an averaging time of 3 seconds was used initially, although 5-sec averaging is now the standard data-taking mode. Integrations of 165 seconds duration are obtained at each of the grid points described above. OBSERVE files are constructed so that during the course of a 10.5 hour run, all the fields at a given declination can be observed. The grid utilized is well-matched to the chosen integration time per field, since the pointing centers are separated in Right Ascension by 3 minutes over most of the sky. Other relevant aspects of the VLA common to *FIRST* and *NVSS* are described in Condon et al. (1994) and will not be repeated here.

Only circular polarization modes are recorded. The survey flux density scale is defined by 3C286 which is assumed to have a flux density of 15.00 Jy at 1365 MHz. The data taking in 1994 has been monitored in quasi-real time by Dr. R. Perley, our collaborator at the VLA site.

The 1993 observations were conducted in a strip near the local zenith; they cover a region defined by $28.2 < \delta < 31.0$, $7^{\rm h}15^{\rm m} < {\rm RA} < 16^{\rm h}30^{\rm m}$ (all coordinates throughout are J2000). A total of 2153 individual fields were observed. The 1994 observing session ran from 4 June through 10 September and includes a total of 483 hours. These $\sim$ 9200 observations extend the strip northward to $\delta = 41.0$ deg in the RA range $7^{\rm h}30^{\rm m}$ to $17^{\rm h}30^{\rm m}$; in addition, about 250 observations from the previous year were repeated to fill in missing data. The exact boundaries of the region covered are shown in FIGURE 5. All of the raw data from these pointings are available to any interested user; the schedule for release of the self-calibrated UV data, the maps, and the catalogs can be found in the *FIRST* home page (see §2.3). The current plan is to continue scheduling *FIRST* observations at 480 hours per configuration cycle in coming years.

6. THE DATA REDUCTION AND ANALYSIS PIPELINE

The primary data stream from the *FIRST* survey consists of 5-second samples of the correlated signal from each of the 351 VLA antenna pairs in each of fourteen 3-MHz frequency channels in each of two circular polarizations, or 324,000 samples of the UV plane per 165-second integration. There are 215 pointings per 10.5-hour day (including calibration observations), or $\sim 10,000$ per season's observing run. This data rate, along with the attendant requirement of eventually producing from these data 65,000 4×10^6 pixel images leads to certain imperatives for the data reduction and analysis pipeline. It must require a minimum of human intervention, and must be able to keep up with the data flow; both objectives must be achieved without compromising the quality of the final maps. Thus, we require a highly reliable, automated system which incorporates optimal editing, calibration, mapping, CLEANing and coadding procedures. We have designed, built, and tested extensively a pipeline system meeting these requirements. The system uses three scripts based on standard AIPS tasks, but incorporates several special-purpose tasks and modifications to standard procedures which we have produced specifically for the pipeline. In this section, we describe the innovative aspects of the pipeline developed for *FIRST*; detailed descriptions of standard AIPS tasks are available in the EXPLAIN files of the AIPS system.

Following standard FILLing of the data from the VLA on-line system, the phase and amplitude calibration is done using the calibration sources observed for this purpose. However, no data editing is carried out prior to pipeline processing. These raw UV data with initial calibrations applied are archived at the VLA and a copy is sent to the Institute for Geophysics and Planetary Physics at Lawrence Livermore National Laboratory (IGPP/LLNL) for pipeline ingest.

Two AIPS tasks, UVLIN and CLIP are used to flag bad visibility data resulting from man-made or natural radio frequency interference, receiver problems, or correlator failure. UVLIN is run twice, once at the outset with a threshold of 5 Jy, and again at the end of the self-calibration loop with a lower threshold, determined with UVPRM and equal to the sum of 10% of the zero-spacing flux plus 4 σ (typically $\sim$ 0.4 Jy). After the first UVLIN run, the task CLIP is run on a channel-by-channel basis with a threshold determined again from UVPRM. For the second pass of UVLIN, the position of the brightest source in the field is used as a temporary phase center, since this facilitates UVPRM's ability to model the data owing to the slower changes in the amplitudes of the UV components. These tasks are highly effective in removing corrupted visibility data. The message files

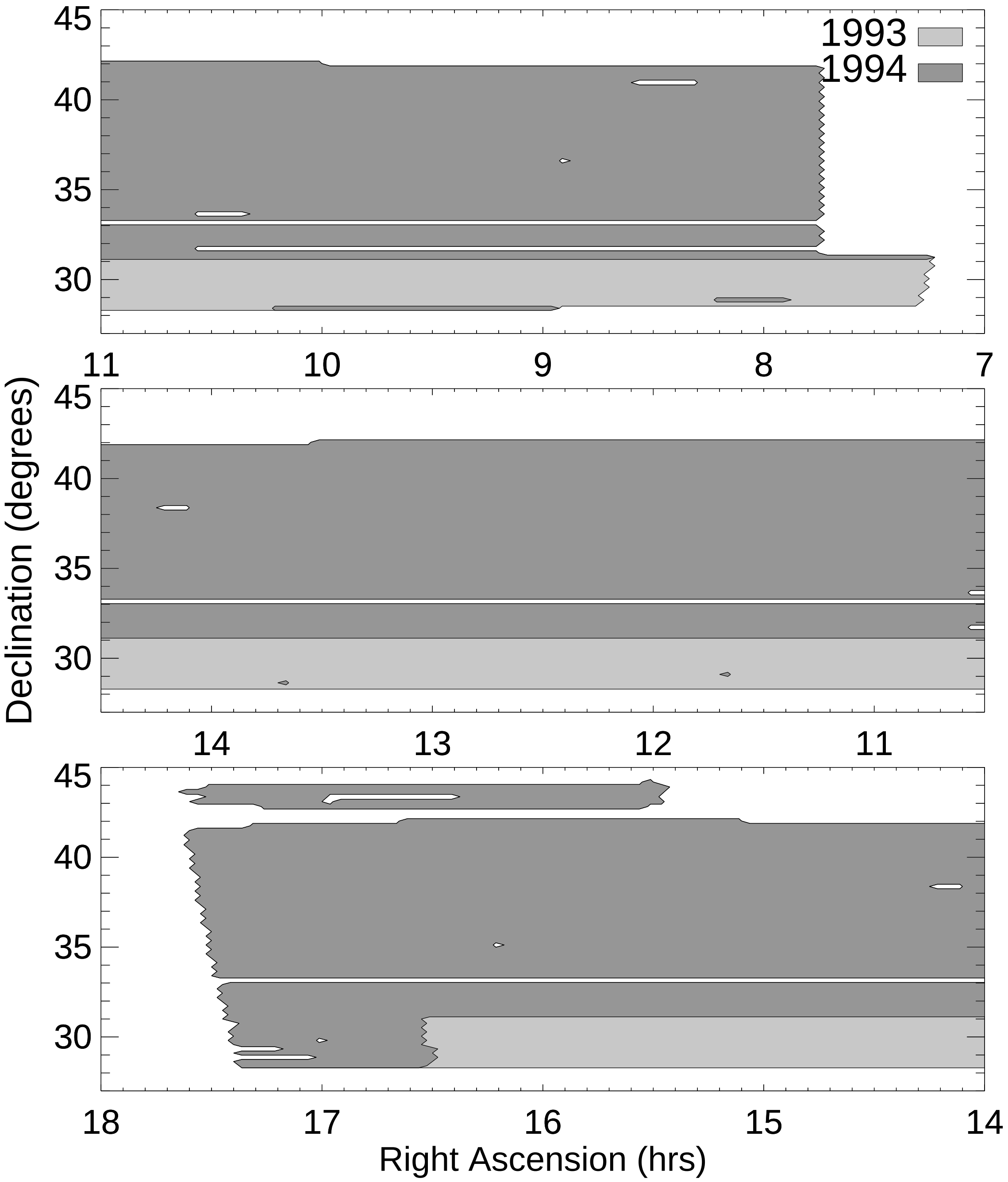

FIGURE 5. Area of sky covered by *FIRST* survey during the 1993 and 1994 observing campaigns. The 1993 observations covered about 300 deg^2, and the 1994 observations covered an additional 1310 deg^2. Only a small fraction of the data ($\sim$ 3%) was lost due to problems during observing.

generated by the two tasks are examined in order to determine for which fields significant ($\gtrsim$ 10%) data loss has occurred; for the 1993 observing season, fewer than 2% of the 2153 fields were affected by interference at this level, and only a small fraction of these require reobservation.

The problem of self-calibrating the visibility data had the potential of requiring unobtainable levels of computational resources. To avoid the necessity of repeatedly creating 2048×2048 images, we have adopted a number of efficient procedures. Before a single image is created, a search of the Green Bank 20 cm and 6 cm catalogs (Becker et al. 1991; White and Becker 1992) finds all sources with $S_{20} > 100$ mJy within 10 degrees of the field center. A tapered map is then produced which includes the full area of the primary beam along with a number of smaller images centered on off-axis sources that, given the primary beam pattern, will appear brighter than 2 mJy. The tapered image as well as the satellite images are then searched for all sources above 2 mJy. The positions and flux densities of these sources are stored in a file for later use (note that these files already constitute a radio source catalog superior to any in existence). With this list of all sources contributing to a field, it is possible to self-calibrate the data with roughly a dozen 32×32 pixel maps, rather than all-encompassing 2048×2048 images. If the tapered map reveals any source brighter than 30 mJy, a three-iteration phase self-calibration is carried out. In most cases, the phase changes resulting from this self-calibration are less than ~ 20 deg.

Before the data are imaged, the task UVFIX is run to improve the accuracy of the astrometric solution. The data are then passed through the task UBAVG which effectively increases the integration time where possible in order to reduce the total number of visibility points without degrading the final image. Natural weighting is used in gridding the UV data.

The final step before constructing the CLEANed image is to shift the center of the map by up to one pixel ($1.8''$) to assure that the brightest source in the image falls precisely at a pixel center. This procedure has been shown to reduce the sidelobe level from the brightest source in the final map. The shift is determined from a dirty map made expressly for this purpose; only fields with sources brighter than 25 mJy undergo this procedure.

A miscentered bright source is only one of the effects that produce avoidable sidelobes in the final image. Two others which we have attempted to avoid result from adding together data collected at several different frequencies. Since the primary beam response is frequency-dependent, a source at the edge of the primary beam where the gradient in the response is steepest can appear very different in the two IFs. Likewise, sources with non-zero spectral indices will also differ between the two frequency bands. Thus, if the two IFs are merged before mapping, the CLEANing process will not succeed in subtracting correctly 100% of the source flux, leaving behind unnecessarily high sidelobes. The obvious solution is to image the two IFs separately, but doing so reduces the UV coverage in the map which leads to larger sidelobes — just what we are trying to avoid. The solution to this dilemma is a compromise which we find produces maps with minimum sidelobe contamination.

Initially, we map and CLEAN the two IFs separately down to a flux density limit of 10 mJy using the newly created task WFCLZ (a modified version of WFCLN). Maps from WFCLZ are then written to disk with all the residuals set to zero. The CLEAN components from each map are subtracted from the visibility data of their respective IFs. The task WFCLN is then run on the two IFs combined until a CLEANing limit of 0.5 mJy is reached or 10,000 CLEAN components have been subtracted, whichever comes first. When this CLEAN is finished, the two earlier maps containing the bright sources are averaged together and added to the third image. Thus, the deep CLEAN is made with the

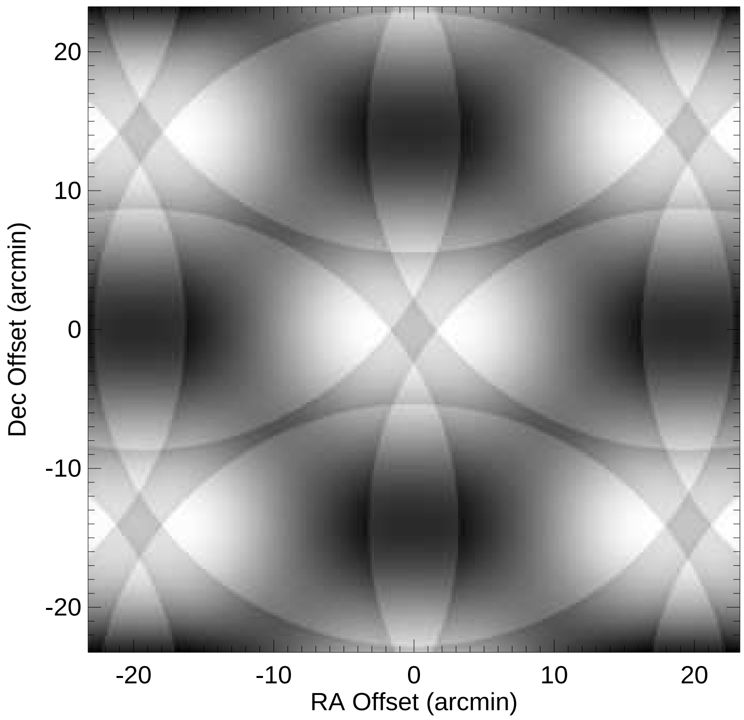

FIGURE 6. Sensitivity as a function of position in the coadded maps at declination $+29°47'$. The noise is higher (so the sensitivity is lower) in the dark regions. The rms noise level in the coadded map ranges from 0.131 to 0.154 mJy/beam.

full UV coverage, while the bright components have not been compromised by differences between the two IFs.

The final map suffers from significant distortion resulting from the use of a two-dimensional FFT to approximate the curved celestial sphere (see Perley 1989 for a full discussion of this effect). This distortion is removed with the task OHGEOM. Another small distortion, due to annual aberration, is removed by changing the pixel size of each map by a small amount (typically 1 part in 10^4). The final images have systematic astrometric uncertainties of $\lesssim 0.05''$.

The final step in the pipeline is to sum adjacent images both in order to obtain better signal to noise and to improve coverage uniformity. In general, each field has significant overlap with 12 other fields in the grid. These 12 maps are truncated at a radius of $23.5'$, weighted by the square of the primary beam response, and summed (see Condon et al. 1994 for a full justification of this procedure). Given the degree of overlap of the pointing grid, complete coadded images need be constructed only for pointing centers in every other declination strip. The resulting coadded images have a peak to peak sensitivity variation of only $\sim 15\%$ over the entire survey region (FIGURE 6) and allow for the detection of up to 50% more sources than are observed in the single field images. The dynamic range of the final images is $\gtrsim 1000:1$.

7. MAP CHARACTERIZATION

We have conducted a number of tests on the survey images and the sources extracted therefrom in order to verify our procedures and establish the survey's accuracy in estimating source parameters. In this section, we briefly outline our progress to date.

We have several means at our disposal to verify information derived from our images:

- we can test our positions against lists of radio interferometer astrometric standards.
- we can insert artificial sources into the real UV data sets using the AIPS task UVMOD and measure what comes out of the end of our pipeline;
- we can compare the results for multiply observed sources (MOS); i.e., sources which, owing to the significant field overlap, are observed in more than one image;
- we can compare our results to those of published deep 20 cm surveys (albeit, over a very limited area of sky);

The results of these tests are presented below.

7.1. *Astrometry*

The accuracy of the *FIRST* positions is excellent. FIGURE 7 presents the observed scatter for MOS sources detected in the 3×3 degree region around the North Galactic Pole (NGP). For sources with flux densities greater than 2 mJy, the reproducibility in individual positions is $\sim 0.4''/\sqrt{2}$ or about one-third of an arcsecond, leading to a 90% confidence error circle with a radius of $\sim 0.5''$. Even for sources at the 1.0 mJy threshold, the 90% error circle is significantly less than $1''$ in radius. To establish that these positions are accurately tied to an astrometric reference frame, we have compared the positions of all MERLIN calibrators found in our 2.8×120 degree strip (46 sources in total) and find an average offset of $< 0.05''$. A detailed discussion of astrometric comparisons with optical positions derived from the APM plate scans will be presented in McMahon et al. (1995); the distribution of optical/radio offsets for over 4100 objects confirms that *FIRST* positions have random errors of $\lesssim 1''$ and systematic errors of $< 0.05''$.

7.2. *Photometry and Completeness*

The primary aims of the B-configuration survey have always been to reach a faint flux density threshold, to obtain high resolution images of extended sources and source complexes, and to achieve optical quality astrometry. Accurate photometry is a secondary goal which, as with all interferometric observations, is necessarily compromised by high angular resolution. Our analysis procedures have been designed to obtain the best possible photometric accuracy for sources with angular extents $\lesssim 5''$ (the synthesized beam size) and to allow for estimation of systematic flux density errors for all sources. For sources substantially larger than the synthesized beam, some flux will inevitably be resolved out, leading to an increase in the survey threshold for extended objects and an underestimate of source intensities for larger objects. Since one of the principal aims of the *NVSS* is accurate photometry on extended and low surface brightness objects, we do not regard this limitation of *FIRST* as a significant problem. Users requiring accurate flux densities for sources whose structure and optical identifications have been found by *FIRST* will be able to consult *NVSS* for photometric information on sources brighter than 2.5 mJy; such information may be included in future versions of *FIRST* catalogs. We will also be exploring the utility of combining the *FIRST* and *NVSS* UV datasets to generate a new set of maps with greater sensitivity to extended objects as soon as some overlap exists between

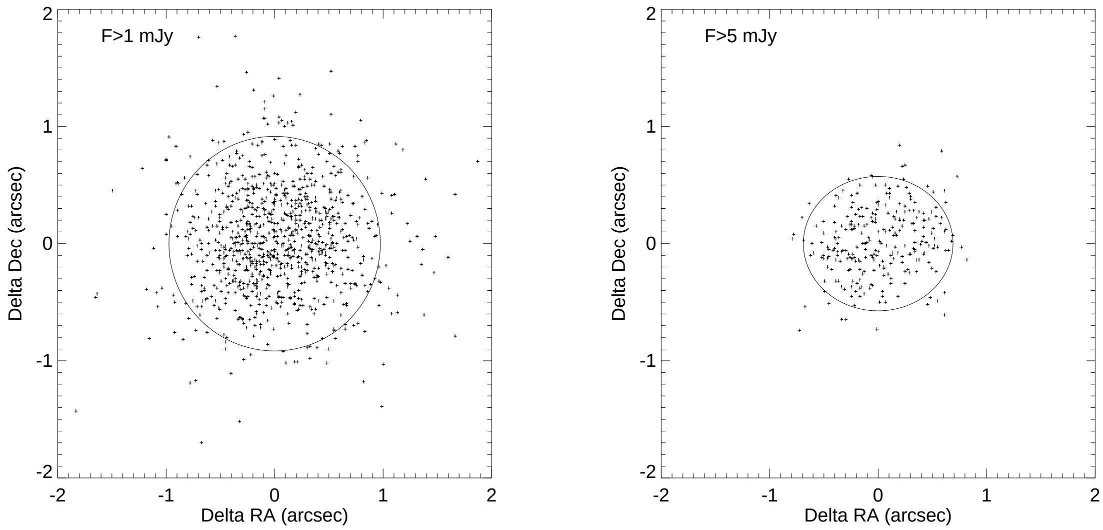

FIGURE 7(A) FIGURE 7(B)

FIGURE 7. Position differences for multiply-observed sources detected in more than one field. This is a strong test of positional accuracy for weak sources. The ellipses show 2 times the rms in RA and Dec. For $F > 1$ mJy the 953 pairs have $0.49''$ and $0.46''$ rms in RA and Dec, respectively, while for $F > 5$ mJy the 267 pairs have rms values $0.34''$ and $0.29''$. Note that both source position measurements are noisy, so the expected rms in the difference is larger than the rms in a single measurement. This test shows that the positions are accurate to $< 1''$ (90% confidence) at the *FIRST* survey flux density limit and that any systematic distortions in the maps are smaller than $0.05''$.

the two surveys (late 1995). Here, we present the photometric properties of the *FIRST* data alone.

"CLEAN bias" is a recently recognized error in the flux densities derived from VLA images. The effect produces a systematic underestimate of flux densities, the magnitude of which is largely independent of the true source flux, and thus affects the weakest sources in a field most severely. The exact cause of this bias is a matter of some debate (see Condon et al. 1994 for one explanation), but the net effect is that the CLEANing algorithm steals flux from discrete sources and spreads it around the image. Using the AIPS task UVMOD to insert artificial sources in our UV data stream, the least ambiguous test available to us for determining the accuracy of the flux densities derived from our images, we find that, for fields in which the brightest source is $\lesssim 50$ mJy ($\sim 50\%$ of all fields), the CLEAN bias is typically $\sim$ 0.25 mJy for point sources, increasing to 1 mJy and 2–4 mJy for sources with diameters of 6 arcsec and 12 arcsec, respectively. The CLEAN bias also increases in maps with higher rms noise levels. For example, for the small number of fields with very bright sources ($>$ 500 mJy; see FIG. 8) in which uncleaned sidelobes can raise the rms by a factor of 2 to 3, this bias can reach 0.5 mJy for point sources and even higher values for extended objects. We have not yet found a way to eliminate this effect, but if we do, we will reanalyze the the data in order to correct it. Also, we are working on a calibration of this effect so that *a posteriori* corrections will be possible for the final source catalog. The results from tests using UVMOD with a range of source sizes and flux densities on a

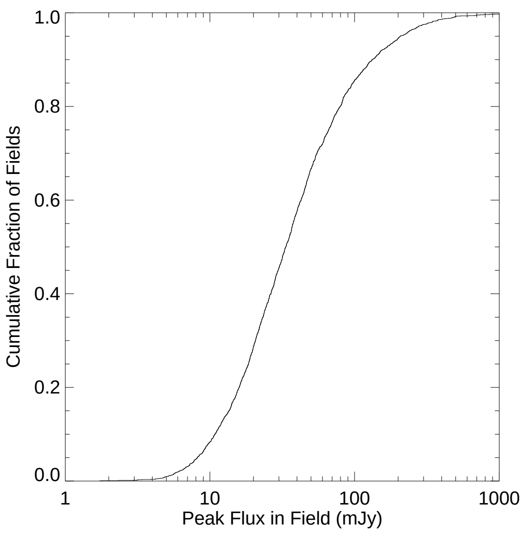

FIGURE 8. Cumulative distribution of maximum flux density for the 2153 fields observed during 1993. The median is 33 mJy with 10% and 90% bounds at 11 and 130 mJy.

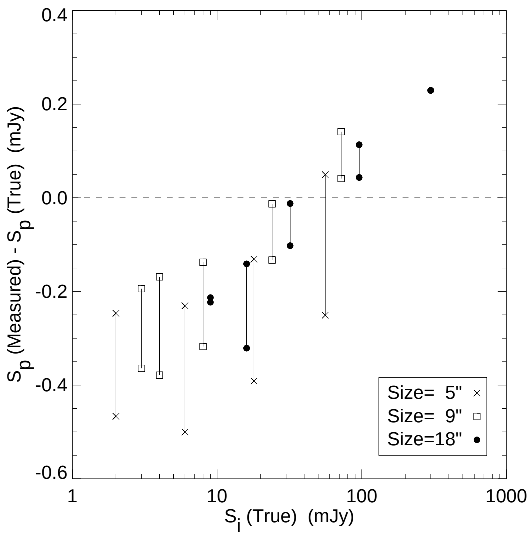

FIGURE 9(A)

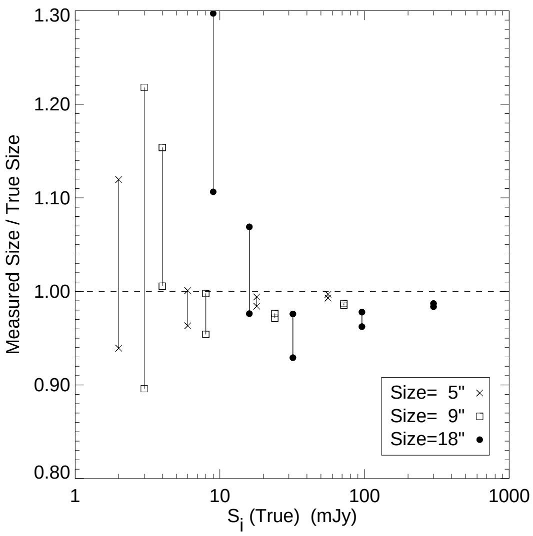

FIGURE 9(B)

FIGURE 9. Results of CLEAN bias tests using artificial sources. (a) Difference between measured peak flux density and true peak flux density as a function of true integrated flux density. Bias is approximately 0.25 mJy; the amount of bias is less for very bright sources. (b) Ratio of measured source size to true size as function of true integrated flux density. The size is determined accurately even for sources considerably larger than the 5.4$''$ *FIRST* synthesized beam.

variety of our UV datasets are given in TABLE 4 and FIG. 9.

The introduction of artificial sources into the UV data also allows us to make a quantitative estimate of the missing flux density resulting from the absence of short spacings in the B configuration. We find that for sources with diameters of 9, 18, 24, and 30 arcsec we are sensitive to 99%, 97%, 84%, and 77%, respectively, of the true source flux density. For most faint sources, however, the CLEAN bias is a greater problem, and is the determining factor is setting the completeness level of the survey

An alternate way to look for CLEAN bias as well as other systematic photometry errors is by comparing flux densities derived for the multiply-observed sources. If all sources in a field suffer from photometric errors prior to the primary beam correction, then after the correction, the error would depend on distance from the field center, and one would expect flux densities for the same object in adjacent fields to differ. Our data show no such effect (see FIG. 10; note that this is also a test of the primary beam correction function, the coefficients of which we have taken from the calibration observations of Condon et al. [1994]). An interesting sidelight of this test is that it also represents the first stage of a search for radio sources which vary on timescales of minutes (from adjacent fields observed the same day) to days (for a source observed on two adjacent strips). It is obvious from FIGURE 10 that variability by a factor of 2 could be recognized to the survey limit and smaller variability could be detected for brighter sources.

The results from comparing our survey images with existing deep interferometric surveys at 20 cm are fraught with sparse overlap and resolution uncertainties. Nonetheless, this is clearly the most meaningful test for photometric accuracy and survey completeness. One published deep VLA pointing is contained in the strip we observed in 1993. A field centered at RA(1950) = 13 00 37, Dec(1950) = 30 34 was observed for $\sim$ 24 hours at 20cm in the C configuration, resulting in an image with an rms of $\sim 11\ \mu$Jy (Mitchell and Condon 1985). The catalog for this field contains 49 sources with integrated flux densities greater than 0.75 mJy, our nominal 5σ threshold. A source-by-source comparison shows that, in the relevant coadded *FIRST* survey image, we detect 100% of the 9 sources with an integrated flux density $>$ 4 mJy, 19 out of 20 of the sources brighter than 2.0 mJy, 71% of the 21 sources between 1 and 2 mJy, and 63% of the 8 sources between 0.75 and 1.0 mJy (FIG. 11). These values are very similar to those expected based on the known distribution of angular sizes for faint sources (see §3.2 and compare column 4 to column 7 and column 6 to column 8 in TABLE 1).

Of the 10 sources not detected in the *FIRST* survey, 7 are clearly very extended in the deep VLA pointing; in fact, they are the 7 sources with the largest values for the peak-to-integrated flux density ratio in the deep survey catalog. These sources have very low peak surface brightnesses as observed by the B-configuration and so are expected to fall below our threshold. Unfortunately, it is not possible to test our source completeness as a function of size quantitatively from the Mitchell & Condon data, because the Mitchell & Condon maps were not corrected for distortions introduced by the non-planar VLA array (see §6), so the sizes inferred from the peak-integrated ratio are systematically overestimated (Condon, private communication). Nonetheless, it is clear that the sources missing from the *FIRST* images are, as expected, only the most extended objects.

On average, we detect 0.38 ± 0.54 mJy per source less than the integrated flux density reported in Mitchell and Condon (1985). Excluding three sources with large discrepancies which could arise either from source variability in the decade between the observations or from small errors in the very large PBCOR values ($\sim$ 10) applied to these particular sources in the deep survey, the mean is reduced to 0.27 mJy, and the median value is 0.22

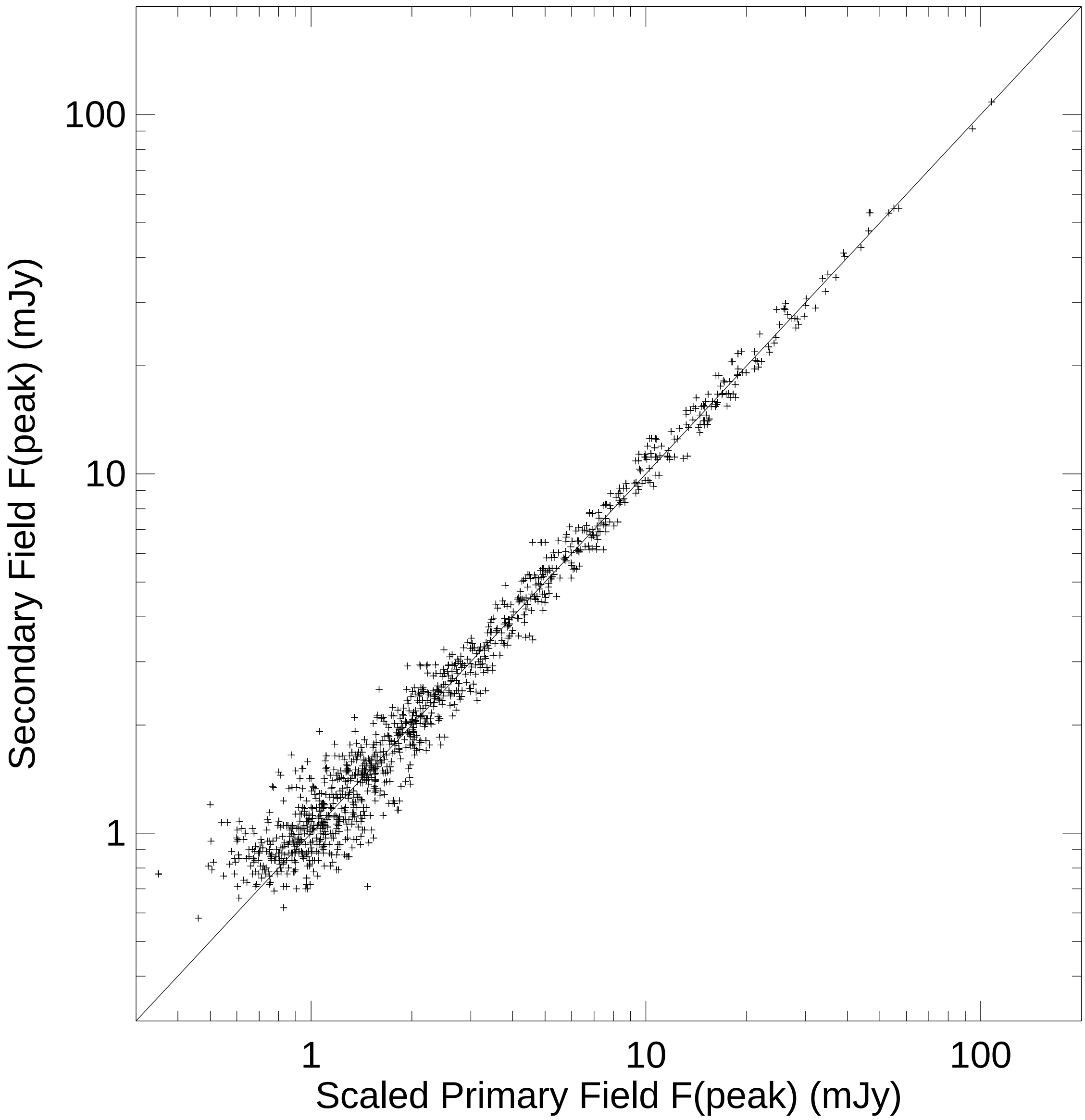

FIGURE 10. Comparison of flux densities for multiply-observed sources. For each of the 1177 pairs of observations, the measured flux density from the primary field (in which the source is closest to field center) is scaled by the ratio of primary beam responses to predict the flux density for the source measured in the secondary field. The excellent agreement indicates that the primary beam response is well-modeled and that systematic errors in the flux densities are small. Note that a large CLEAN bias would cause the distribution to fall below the line at low flux levels; the observed distribution is consistent with a CLEAN bias of 0.25 mJy, but rules out a CLEAN bias as large as 0.35 mJy.

mJy. This mean value is the same as that derived from the insertion of artificial sources into our maps (see §3.2). We conclude from this comparison that our CLEAN bias for point sources is indeed ~ 0.25 mJy.

The impact on the overall source counts of both resolution and our uncertainty about the magnitude of CLEAN bias effects is not large: a comparison of our dN/dS distribution

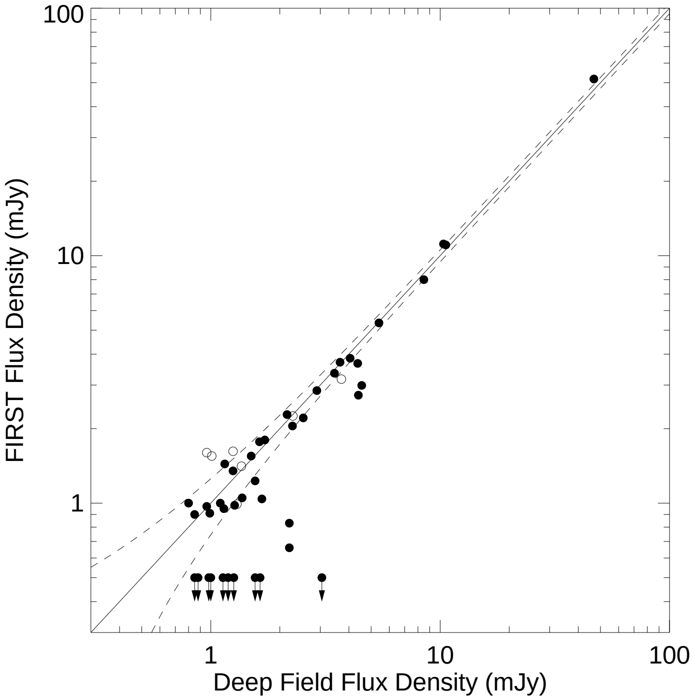

FIGURE 11. Comparison of *FIRST* flux densities with measurements of the 49 sources brighter than 0.75 mJy from the deep survey field of Mitchell & Condon (1985). A CLEAN bias correction of 0.25 mJy has been added to all *FIRST* flux densities. Most sources have *FIRST* flux densities consistent with the deep survey fluxes to within errors expected from map noise and < 5% calibration uncertainties (dashed lines.) Extended *FIRST* sources (FWHM = 4 to 12 arcsec), plotted with open circles, have peak flux densities as small as 0.3 mJy/beam; Malmquist bias causes faint extended sources measured by *FIRST* to be systematically too bright, since fainter sources could not be detected in the *FIRST* map. Deep survey sources not seen in the *FIRST*map are marked with arrows; these are extended sources with peak flux densities too low to be detected in our B-configuration snapshots. Only about 10% of the detected sources show evidence that a significant fraction of the flux has been "resolved out" by our B-configuration observations.

for the 1993 data with that of Windhorst et al. (1985) shows excellent agreement in both slope and normalization to < 2.0 mJy (FIG. 12).

7.3. *Morphology*

The ability of *FIRST* to resolve radio source structure down to a few arcseconds in size is a facet of the survey which may prove to be of great significance in source classification. FIG. 13 graphically illustrates the improvement over existing work. As a more quantitative measure of the advantage the $5''$ beam size of the B configuration confers, we have determined from our preliminary catalog of 28,000 entries the number of sources that will be resolved by *FIRST* but will appear point-like to the $45''$ beam of the *NVSS*. Adopting a flux density threshold of 2.5 mJy for the latter survey (Condon et al. 1994), this region of sky will yield $\sim 12,000$ NVSS sources. These include both discrete isolated sources above the 2.5 mJy threshold and multiple sources that fall within one NVSS beam and have a total flux density > 2.5 mJy. This source list includes 3000 doubles, 650 triples, 230 objects with more than three components, and 2500 other sources with angular sizes

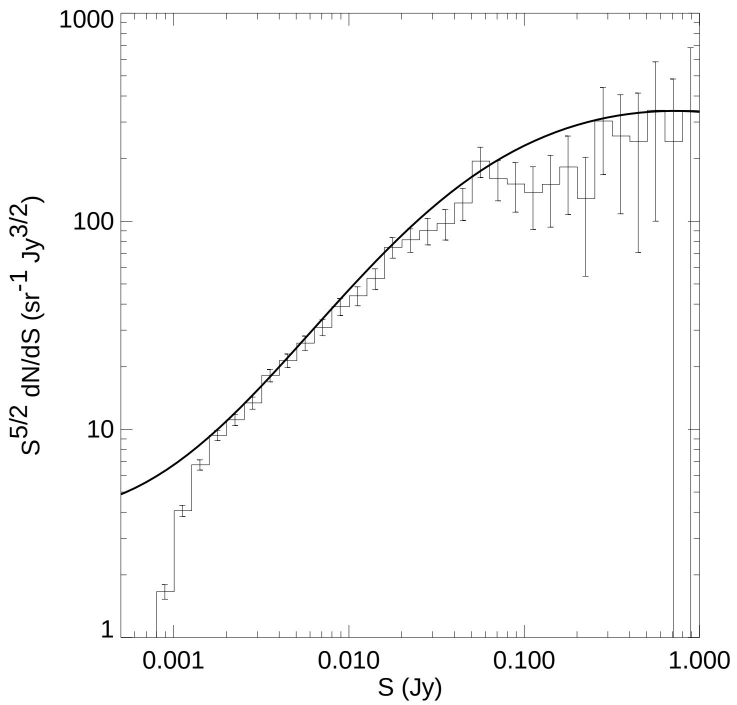

FIGURE 12. Source number density, dN/dS, versus flux density S at 20 cm for *FIRST* data (histogram) compared with previous observations (thick line; Condon 1984, Windhorst 1985). The *FIRST* flux densities for 2874 sources are from a preliminary catalog covering 31.3 deg^2 (RA = 8^h–10^h, Dec = 29.2°–30.3°). To correct for CLEAN bias, 0.25 mJy was added to each integrated flux density measurement. The *FIRST* counts decline below about 1.5 mJy because a significant fraction of weak extended sources have peak flux densities that fall below our detection threshold; for brighter sources the agreement is excellent.

$2.5'' < \theta < 25''$ (resolvable by *FIRST* but not by the NVSS.) Thus, *FIRST* will be able to provide important morphological information on 55% (6,400 of 12,000) of the NVSS "point source" catalog entries. FIG. 14 shows a few examples from a single *FIRST* field in the form of the postage stamps we generate for each source in the catalog.

Tests to date indicate that the fitted source size parameters are quite accurate. We have found that the major and minor axes of sources derived from adjacent fields is generally in very good agreement (see FIG. 15). In addition, from our experiments with artificial sources, we find that, for sources with flux densities $\gtrsim 5$ mJy, we recover size estimates accurate to better than 10% despite the fact that, as described above, CLEAN bias and overresolution of extended sources compromise photometric accuracy. Much work remains to be done, however, in exploring algorithms for quantifying overresolution effects on extended objects, associating multiple components of complex sources automatically, and defining likely positions for optical counterparts for extended and multiple-component objects.

7.4. *Noise Level*

In FIG. 16A, we plot the rms noise level determined from the 2153 individual maps constructed from the 1993 observations; FIG. 16B shows the integral distribution. Greater

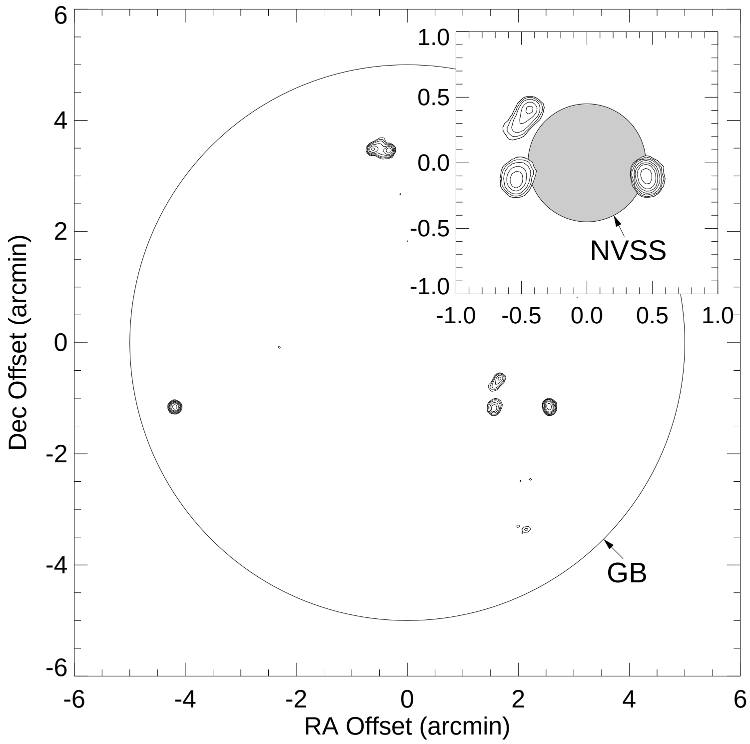

FIGURE 13. A contour map of a portion of a *FIRST* survey image with the FWHM of the Green Bank 300-ft telescope 20 cm beam superposed. The inset shows a small part of this field with the NVSS synthesized beam size. The map center is RA = $13^{\rm h}00^{\rm m}37.8^{\rm s}$, Dec = $+29^\circ41'14.9''$; contour levels are 0.5, 1, 2, 5, 10, 20, and 50 mJy/beam.

than 97% have values $< 150\,\mu$Jy; the coadded images have an even higher fraction of fields for which a peak flux density threshold of 0.75 mJy represents $> 5\sigma$. The increase in both the mean and the scatter for fields containing bright sources results from incomplete CLEANing of sidelobes in these snapshot images. We are exploring the value of treating all fields with sources brighter than, say, 300 mJy, individually, as well as developing a source detection algorithm which flags potential sidelobes based on their azimuthal distribution in the map.

8. THE SOURCE CATALOG

A typical coadded *FIRST* image covering 0.41 deg^2 contains 1.8 x 10^6 pixels but only $\sim$ 40 discrete radio sources above a threshold of 0.75 mJy. Thus, while the maps are a valuable resource as an archival image of the radio sky, as well as for such tasks as deriving upper limits to sources found at other wavelengths, the most useful scientific product of the survey is the source catalog. Given the nonuniform noise characteristics in coadded snapshot images (see FIG. 17) and the large variety of morphologies exhibited by various radio source populations, automatic extraction of a highly reliable and complete catalog from the *FIRST* images is a nontrivial task. However, because of its scientific importance for users, as well as the central role it plays in characterizing image quality and integrity, we have expended considerable effort in developing algorithms to produce a source catalog. We expect to continue these efforts for some time to come. Nonetheless, we now have a

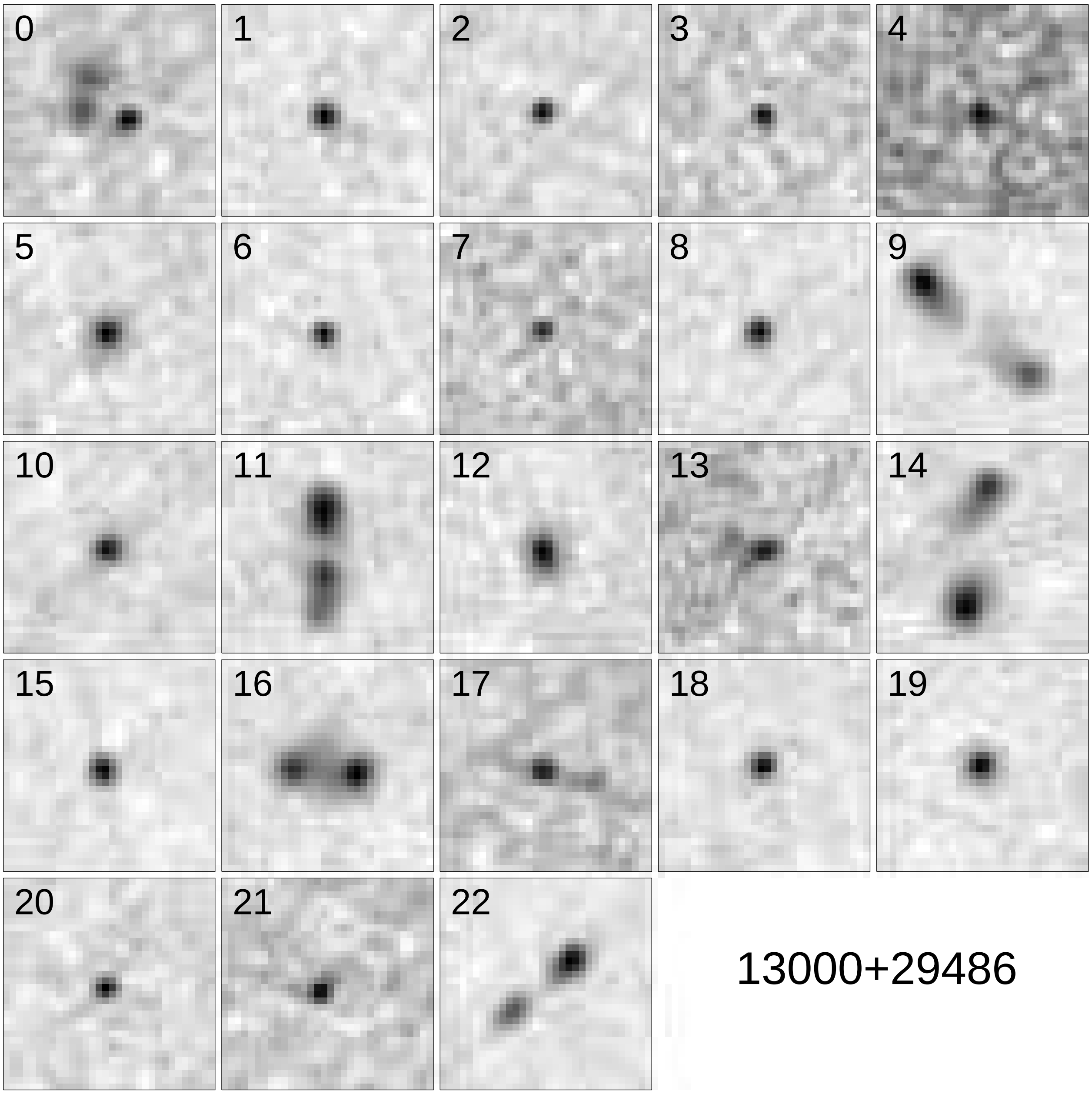

FIGURE 14. A set of postage stamp images from one of our 1993 fields. Each image consists of a grayscale representation (scaled to the brightest point in that image) of a 32 x 32 pixel (1.8 arcsec per pixel) section of the coadded map 13000+29486; each image is approximately the size of the NVSS beam. Only four of the sources in this 0.25 square degree field have been previously catalogued and none of the double sources (which are recorded as separate entries in our catalog) has been resolved. The faintest source (number 4) has a peak flux density of 0.80 mJy, and the brightest (source 12) has an integrated flux density of 132 mJy; this latter source has a measurable extent of 5.4 arcsec in the north-south direction. The components of source 22 have a combined integrated flux density of 9.8 mJy. Images such as these have been created for all 28,000 sources in the 1993 data set on a field by field basis; access instructions are available on the *FIRST* homepage.

functioning source extraction program which has generated a preliminary catalog from the 1993 dataset containing 27,680 entries; this catalog can be retrieved via the *FIRST*

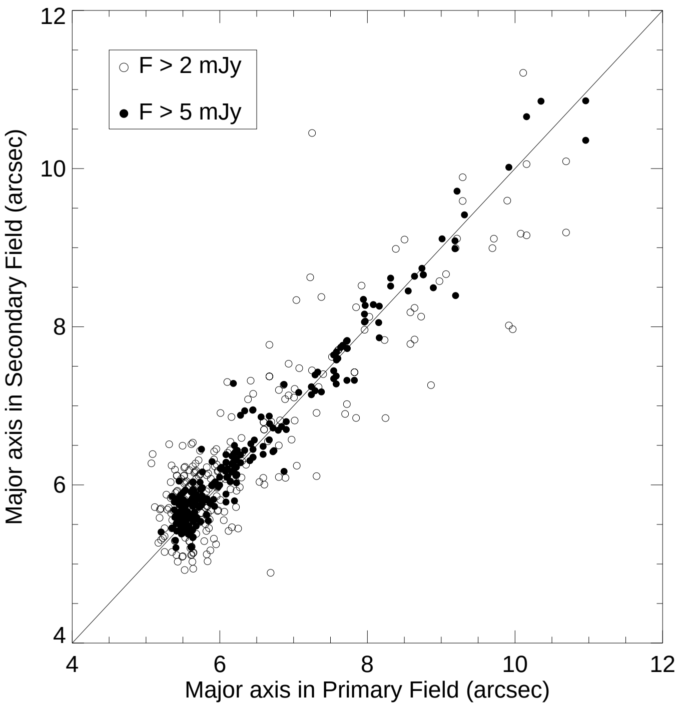

FIGURE 15. Comparison of major axis FWHM for multiply-observed sources. Filled symbols indicate sources with apparent flux densities greater than 5 mJy in both fields, while open symbols include sources as faint as 2 mJy. The rms difference in sizes is $0.44''$ for $F > 2$ mJy and $0.23''$ for $F > 5$ mJy. Point sources cluster around the $5.4''$ synthesized beam width, which has not been removed from the measured sizes.

home-page where a more detailed description can be found. A paper describing the catalog construction process is in preparation (White et al. 1995).

9. Scientific Impact of the Survey

The most important discoveries that have been made using the POSS — quasars, starburst galaxies, the large-scale structure of the Universe — were not anticipated by those who carried out the original survey. And many of these discoveries have come as a result of comparing work done at other wavelengths with this unparalleled optical database. Likewise, we cannot anticipate all of the new source classes and astrophysical insights that the *FIRST* survey will yield, but we are confident that cross-correlation of the maps and catalogs we produce with data from other wavelength regimes will be enormously productive. To maximize the utility of the survey, it has been designed to cover the same 10^4 square degrees of sky as the Sloan Digital Sky Survey (SDSS) which will, by the end of the decade, have produced five-color CCD images of this entire area to $m_v = 24$ and will be in the process of collecting spectra from 10^6 of the objects therein. The subarcsecond positions our survey will produce will allow immediate optical identification of $> 50\%$ of our radio catalog from the SDSS database, further enhancing its utility. While an exhaustive description of the scientific impact this project will have is beyond the scope of this paper, a few examples of areas in which the *FIRST* survey will make fundamental contributions include:

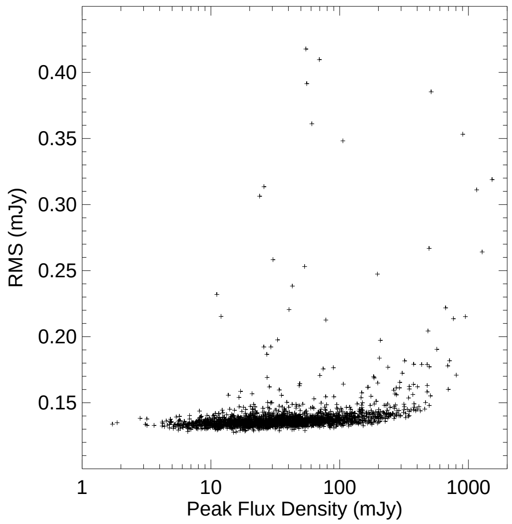

FIGURE 16(A)

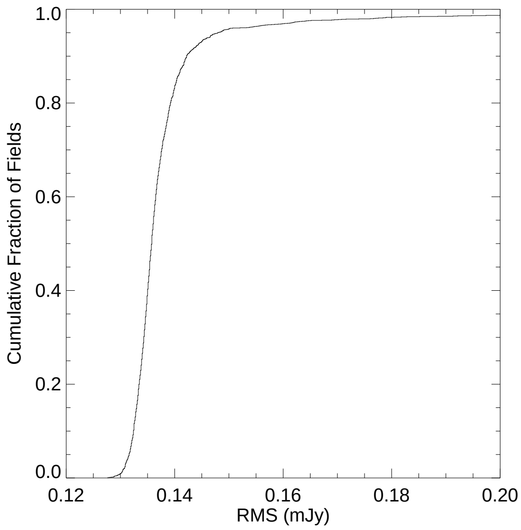

FIGURE 16(B)

FIGURE 16. (a) Distribution of rms noise level for the 2153 fields observed during 1993 in maps produced with the automated *FIRST* analysis pipeline. Only a very small fraction of the fields is limited either by dynamic range (because there is a bright source in the field) or by the inability to clean complex sources. (b) Cumulative distribution of rms noise: fraction of fields that exceed given noise level. Fewer than 5% of the fields have rms noise levels 10% above the median rms (0.136 mJy).

- the evolution of radio-loud quasars from a complete, flux-limited sample of 20,000 such objects brighter than $B = 19.5$;
- quasar absorption line studies from the sample of several hundred new quasars brighter than $B = 17$;
- the bivariate X-ray-radio luminosity function for BL Lacs through an increase in the sample of known BL Lacs by a factor of ~ 30 via cross-correlation with *ROSAT* catalogs;
- unified models of AGN, in that complete flux-limited samples of all classes of active nuclei (Seyferts, BL Lacs, OVVs, radio galaxies, and quasars) with $\sim 10^3$ to $\sim 10^5$ members each will emerge from the comparison of this survey with the SDSS AGN sample;
- the evolution of the intracluster medium of galaxy clusters through the identification of large samples of distant clusters using head-tail and bent-jet radio sources as tracers;
- the evolution of large-scale structure through the use of complete flux-limited samples of radio galaxies and/or starburst galaxies discovered in the survey, as well as the statistics of the radio source spatial distribution and cross-correlation with microwave background fluctuation studies;
- gravitational lenses, by discovering radio arcs, lensed radio galaxy lobes, and multiple point sources through the use of various optical filters;
- galaxy evolution from a variety of perspectives including the followup of high redshift, steep spectrum radio galaxies, and the identification of objects such as IRAS

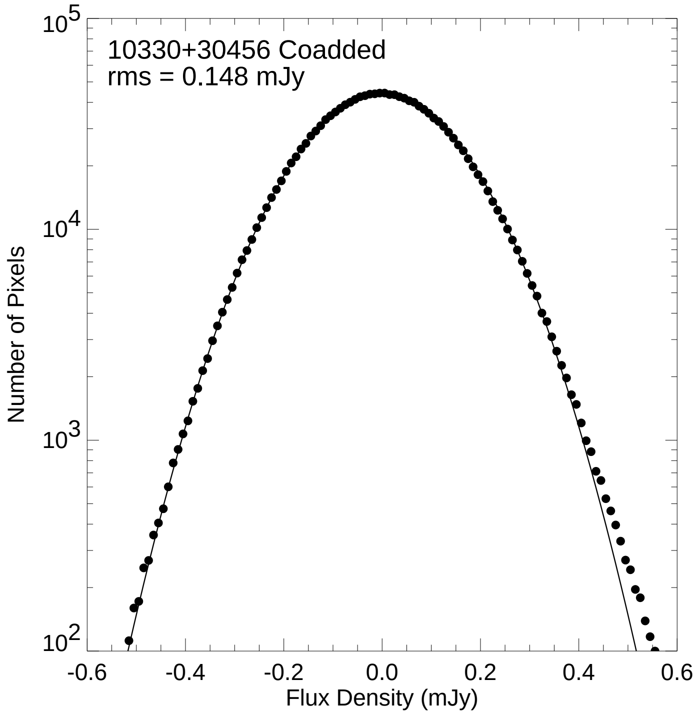

FIGURE 17. The distribution of pixel values in the coadded image for the field 10330+30456. The smooth curve represents a Gaussian distribution with $\sigma = .148$ mJy. The noise closely approximates a Gaussian. The excess at positive values represents primarily the detection of faint sources: we expect ~ 100 sources per .3 square degree image, each covering several pixels, at the 3σ level of ~ 0.4 mJy.

10214+4724 (a source below the *NVSS* threshold) from comparison with IRAS and ISO samples;

- the discovery of nearby millisecond and normal pulsar candidates through the identification of steep spectrum objects using the Texas and Westerbork Northern Sky Survey catalogs in the first wide-area survey unbiased with respect to low duty cycles, high dispersion measures, short periods, and large binary accelerations;
- through the comparison of large stellar catalogs directly with the maps, the first radio-selected samples of stars with a flux density limit of 0.5 mJy for use in such diverse applications as the identification of nearby, coeval moving groups of red dwarfs and the prevalence of magnetically active coronae on all late-type stars;
- the inevitable new phenomena that emerge when one addresses such a large region of hitherto unexplored parameter space.

10. Public access to the FIRST Survey

The *FIRST* images and catalogs represent an important new resource for the world-wide astronomical community, and we are anxious to provide access to all astronomers with an interest in using them. As noted above, we have waived the normal proprietary period for all *FIRST* data; thus, the complete set of raw UV data for both the 1993 and 1994 observing runs are available now from the VLA. We have also completed the editing and self-calibration step for all these data, and the files for all $\sim 11,400$ observations are also now available from the NRAO. To provide optimal access to the images, postage stamps, and catalogs, we will be installing them in several commonly used archives. The STScI DADS system is now ingesting all of the individual field maps as well as the coadded images from 1993; the coadded images have been available on-line since late 1994. NRAO also has a complete copy of the coadded images. The source catalog and postage stamp images are being put on line at NRAO, at STScI, at the High Energy Astrophysics Science Archive Research Center (HEASARC), and as part of the NED system at IPAC. Detailed instructions for accessing *FIRST* results as well as a current status report for the survey may be found via the *FIRST* homepage (http://sundog.stsci.edu/).

Acknowledgements

This major undertaking has received generous technical and scientific support from many individuals. The NRAO staff has provided extremely valuable assistance in many aspects of the observations themselves and in the area of software support; in particular, we are grateful to Rick Perley, Ken Sowinski, Barry Clark, and Bill Cotton in this regard. The support of the NRAO Director, Paul van den Bout, and the yeoman service provided by Frazer Owen as Chair of the Survey Oversight Committee are also greatly appreciated. We also thank the members of the Oversight Committee (Ken Chambers, Eric Feigelson, Jackie Hewitt, Gillian Knapp, and Rogier Windhorst) for their time and wise counsel in this enterprise. Pat Crane is acknowledged for his professional supervision of the observations during the 1993 run. Acknowledgement is also due our colleagues who are involved in the ongoing *FIRST* effort, including Richard McMahon, Michael Gregg, Yihan Fang and Rick Perley. This work was supported in part under the auspices of the Department of Energy by Lawrence Livermore National Laboratory under contract No. W-7405-ENG-48 and by the Institute for Geophysics and Planetary Physics whose director Charles Alcock has been particularly supportive. We also acknowledge a generous planning grant from the CalSpace Institute, support from the STScI archive group and STScI Director Bob Williams, computing resources from Columbia University, and a recently announced award from the National Geographic Society which, in the spirit of their support 40 years ago for the Palomar Observatory Sky Survey, will be providing funds to continue our charting of the Universe.

This is Contribution Number 555 of the Columbia Astrophysics Laboratory.

References

Bahcall, J.N., & Soneira, R.M. 1980, ApJSupp 44, 73

Becker, R.H., White, R.L., & Edwards, A.L. 1991, ApJS, 75, 1

Becker, R.H., White, R.L., Helfand, D.J., & Zoonematkermani, S. 1994, ApJS, 91, 347

Benn, C.R., Rowan-Robinson, M., McMahon, R.G., Broadhurst, T.J., and Lawrence, A. 1993, MNRAS, 263, 98

Condon, J.J. 1984, ApJ, 287, 461

Condon, J.J. 1992, Ann. Rev. A. Ap., 30, 575

Condon, J.J. & Broderick, J.J. 1985, AJ, 90, 2540

Condon, J.J. & Broderick, J.J. 1986, AJ, 91, 1051

Condon, J.J., Broderick, & Seielstad, G.A. 1989, AJ, 97, 1064

Condon, J.J., Cotton, W.D., Greisen, E.W., Yin, Q.F., Perley, R.A., & Broderick, J.J. 1994, ApJ (in press)

Donnelly, R.H., Partridge, R.B., and Windhorst, R.A. 1987, ApJ, 321, 94

Gregory, P.C. & Condon, J.J. 1991, ApJS, 75, 1011

Gunn, J.E. & Knapp, G.R. 1992, PASP, 43, 267

Harwitt, M. 1981, *Cosmic Discovery* (Sussex: Basic Books)

Helfand, D.J., Zoonematkermani, S., Becker, R.H., & White, R.L. 1992, ApJS, 80, 211

Kellerman, K. & Sheets, J. 1983, *Serendipitous Discoveries in Radio Astronomy* (Green Bank: NRAO)

Kleinmann, S. 1992, in *Robotic Telescopes in the 1990's*, ed. A.V. Filippenko (San Francisco: ASP), p. 203

Koo, D. C., & Kron, R. G. 1992, ARAA 30, 613

Kron, R.G., Koo, D.C., & Windhorst, R. 1985, AAp, 146, 38

McMahon, R.G. et al. 1995, in preparation

Mitchell, K.J. & Condon, J.J. 1985, AJ, 90, 1957

Owen, F., Burns, J.O., Rudnick, L., & Greisen, E.W. 1979, ApJL, 229, L59

Perley, R.A. 1989 in *Synthesis Imaging in Radio Astronomy*, ASP Conference Proc. 6, eds. R.A. Perley, F.R. Schwaab, & A.H. Bridle, p. 259

Reber, G. 1944, ApJ, 100, 279

Soucail, G. 1991 in *Clusters and Superclusters of Galaxies*, ed. A.C. Fabian, (Dordrecht: Kluwer), p. 198

Thuan, T.X. & Condon, J.J. 1987, ApJL, 322, L9

Windhorst, R.A., Miley, G.K., Owen, F.N., Kron, R.G., & Koo, D.C. 1985, ApJ, 289, 494

Windhorst, R., Mathis, D., & Neuschaefer, L. 1990 in *Symposium on the Evolution of the Universe of Galaxies–Hubble Centennial Symposium*, ed. R.G. Kron (San Francisco: ASP), Conf. Ser. Vol. 10, 389

White, R.L. & Becker, R.H. 1992, ApJS, 79, 331

White, R.L., Becker, R.H., Fang, Y., Gregg, M.D., & Helfand, D.J. 1995, in preparation

Wright, A.E., Griffith, M.R., Burke, B.F., & Ekers, R.D. 1994, ApJS, 91, 111

Windhorst, R.A., Miley, G.K., Owen, F.N., Kron, R.G., & Koo, D.C. 1985, ApJ, 289, 494

Zoonematkermani, S., Helfand, D.J., Becker, R.H., & White, R.L. 1990, ApJS, 74, 181

Table 1

Angular Size Distribution and Source Detectability

Integrated[a] Flux Density (mJy) (1)	$\psi_{\rm med}$ ($''$) (2)	$\psi_{\rm crit}$ [b] ($''$) (3)	$1 - h(\psi_{\rm crit})$[c] (%) (4)	Integrated[a] Flux Density (mJy) (5)	LBDS[d] Sources (6)	VLA Deep Survey[e] $F_p > 0.75$ (7)	$> 5\sigma$ in map (8)
30	5.6	30	86	15–50	35/35 (100%)	1/1 (100%)	1/1 (100%)
10	4.0	18	83	5–15	46/47 (98%)	4/4 (100%)	4/4 (100%)
3	2.8	9	76	2–5	46/48 (96%)	10/15 (67%)	14/15 (93%)
1	2.0	1	36	1–2	19/28 (68%)	8/21 (38%)	15/21 (71%)
				0.75–1		0/8 (0%)	5/8 (63%)

[a] Actual source integrated flux density.

[b] Size at which a source with the *integrated* flux density in column 1 falls below a *peak* flux density threshold of 0.75 mJy.

[c] The fraction of all sources expected to be detected above a peak flux density of 0.75 mJy.

[d] Numbers of sources that would be detected by *FIRST*/total sample (and fraction) (from Oort et al. 1987 and Oort 1988).

[e] Mitchell and Condon (1985) detected 49 sources with *integrated* flux densities > 0.75 mJy; we show here the numbers (and fractions) detected using a peak flux density threshold of > 0.75 mJy (column 7) and in a direct query of the maps using IMEAN and a 5σ threshold (column 8).

Table 2
Declination Strips

Declination range	*NRA*[1]	*NDec*[2]	*Nfield*[3]
+89 42.4 to +90 00.0	5	2	6
+88 34.9 to +89 24.8	15	4	60
+86 58.4 to +88 21.3	30	6	180
+82 43.4 to +86 44.7	60	16	960
+74 59.5 to +82 31.1	120	30	3600
+58 27.6 to +74 47.4	240	64	15360
−42 01.0 to +58 15.5	480	418	200640
		Total =	220806

[1]Number of equally spaced RA points in each declination row.
[2]Number of Dec rows in strip.
[3]Total number of field centers in strip ($NRA \times NDec$ except for the zone at the pole, which has only a single point at $+90°$.)

Table 3
Pointing Positions (J2000)

Num	*Dec*	*NRA*	*Num*	*Dec*	*NRA*	*Num*	*Dec*	*NRA*
000	+90 00.0	1	035	+80 11.9	120	070	+70 38.9	240
001	+89 42.4	5	036	+79 54.8	120	071	+70 21.3	240
002	+89 24.8	15	037	+79 38.6	120	072	+70 03.7	240
003	+89 06.7	15	038	+79 22.4	120	073	+69 46.6	240
004	+88 48.5	15	039	+79 06.9	120	074	+69 29.6	240
005	+88 34.9	15	040	+78 51.4	120	075	+69 13.0	240
006	+88 21.3	30	041	+78 36.5	120	076	+68 56.4	240
007	+88 02.1	30	042	+78 21.5	120	077	+68 40.2	240
008	+87 42.8	30	043	+78 06.9	120	078	+68 24.0	240
009	+87 27.5	30	044	+77 52.4	120	079	+68 08.2	240
010	+87 12.1	30	045	+77 38.3	120	080	+67 52.3	240
011	+86 58.4	30	046	+77 24.1	120	081	+67 36.8	240
012	+86 44.7	60	047	+77 10.4	120	082	+67 21.2	240
013	+86 21.6	60	048	+76 56.6	120	083	+67 05.9	240
014	+85 58.5	60	049	+76 43.2	120	084	+66 50.6	240
015	+85 39.7	60	050	+76 29.7	120	085	+66 35.6	240
016	+85 20.9	60	051	+76 16.5	120	086	+66 20.5	240
017	+85 04.5	60	052	+76 03.2	120	087	+66 05.7	240
018	+84 48.0	60	053	+75 50.1	120	088	+65 50.9	240
019	+84 32.9	60	054	+75 37.0	120	089	+65 36.3	240
020	+84 17.7	60	055	+75 24.3	120	090	+65 21.7	240
021	+84 03.4	60	056	+75 11.6	120	091	+65 07.3	240
022	+83 49.1	60	057	+74 59.5	120	092	+64 52.8	240
023	+83 35.6	60	058	+74 47.4	240	093	+64 38.6	240
024	+83 22.0	60	059	+74 24.1	240	094	+64 24.3	240
025	+83 08.9	60	060	+74 00.7	240	095	+64 10.3	240
026	+82 55.7	60	061	+73 38.1	240	096	+63 56.2	240
027	+82 43.4	60	062	+73 15.5	240	097	+63 42.4	240
028	+82 31.1	120	063	+72 54.5	240	098	+63 28.5	240
029	+82 08.4	120	064	+72 33.4	240	099	+63 14.8	240
030	+81 45.7	120	065	+72 13.5	240	100	+63 01.1	240
031	+81 25.7	120	066	+71 53.5	240	101	+62 47.5	240
032	+81 05.6	120	067	+71 34.5	240	102	+62 33.9	240
033	+80 47.3	120	068	+71 15.4	240	103	+62 20.5	240
034	+80 29.0	120	069	+70 57.2	240	104	+62 07.0	240

Table 3 (cont.)
Pointing Positions (J2000)

Num	*Dec*	*NRA*	*Num*	*Dec*	*NRA*	*Num*	*Dec*	*NRA*
105	+61 53.7	240	140	+51 39.6	480	175	+41 29.1	480
106	+61 40.3	240	141	+51 20.0	480	176	+41 13.2	480
107	+61 27.0	240	142	+51 00.3	480	177	+40 57.5	480
108	+61 13.7	240	143	+50 41.1	480	178	+40 41.7	480
109	+61 00.5	240	144	+50 21.8	480	179	+40 26.1	480
110	+60 47.3	240	145	+50 02.9	480	180	+40 10.4	480
111	+60 34.2	240	146	+49 44.0	480	181	+39 54.9	480
112	+60 21.0	240	147	+49 25.5	480	182	+39 39.3	480
113	+60 08.0	240	148	+49 06.9	480	183	+39 23.9	480
114	+59 55.0	240	149	+48 48.7	480	184	+39 08.4	480
115	+59 42.2	240	150	+48 30.4	480	185	+38 53.1	480
116	+59 29.4	240	151	+48 12.4	480	186	+38 37.7	480
117	+59 16.8	240	152	+47 54.4	480	187	+38 22.4	480
118	+59 04.2	240	153	+47 36.7	480	188	+38 07.1	480
119	+58 51.9	240	154	+47 18.9	480	189	+37 51.9	480
120	+58 39.6	240	155	+47 01.4	480	190	+37 36.7	480
121	+58 27.6	240	156	+46 43.9	480	191	+37 21.6	480
122	+58 15.5	480	157	+46 26.6	480	192	+37 06.5	480
123	+57 51.9	480	158	+46 09.3	480	193	+36 51.4	480
124	+57 28.2	480	159	+45 52.2	480	194	+36 36.4	480
125	+57 04.9	480	160	+45 35.1	480	195	+36 21.4	480
126	+56 41.5	480	161	+45 18.2	480	196	+36 06.5	480
127	+56 18.4	480	162	+45 01.3	480	197	+35 51.6	480
128	+55 55.3	480	163	+44 44.6	480	198	+35 36.7	480
129	+55 32.6	480	164	+44 27.8	480	199	+35 21.9	480
130	+55 09.8	480	165	+44 11.3	480	200	+35 07.1	480
131	+54 47.5	480	166	+43 54.7	480	201	+34 52.3	480
132	+54 25.1	480	167	+43 38.3	480	202	+34 37.6	480
133	+54 03.6	480	168	+43 21.9	480	203	+34 22.9	480
134	+53 42.0	480	169	+43 05.6	480	204	+34 08.2	480
135	+53 21.2	480	170	+42 49.3	480	205	+33 53.6	480
136	+53 00.3	480	171	+42 33.1	480	206	+33 38.9	480
137	+52 40.0	480	172	+42 17.0	480	207	+33 24.3	480
138	+52 19.6	480	173	+42 01.0	480	208	+33 09.7	480
139	+51 59.6	480	174	+41 45.0	480	209	+32 55.2	480

Table 3 (cont.)
Pointing Positions (J2000)

Num	*Dec*	*NRA*	*Num*	*Dec*	*NRA*	*Num*	*Dec*	*NRA*
210	+32 40.7	480	245	+24 28.8	480	280	+16 37.7	480
211	+32 26.3	480	246	+24 15.1	480	281	+16 24.4	480
212	+32 11.8	480	247	+24 01.5	480	282	+16 11.1	480
213	+31 57.4	480	248	+23 47.8	480	283	+15 57.8	480
214	+31 43.0	480	249	+23 34.2	480	284	+15 44.5	480
215	+31 28.7	480	250	+23 20.6	480	285	+15 31.3	480
216	+31 14.3	480	251	+23 07.0	480	286	+15 18.0	480
217	+31 00.0	480	252	+22 53.4	480	287	+15 04.8	480
218	+30 45.6	480	253	+22 39.8	480	288	+14 51.5	480
219	+30 31.3	480	254	+22 26.3	480	289	+14 38.3	480
220	+30 17.0	480	255	+22 12.8	480	290	+14 25.0	480
221	+30 02.8	480	256	+21 59.2	480	291	+14 11.8	480
222	+29 48.6	480	257	+21 45.7	480	292	+13 58.5	480
223	+29 34.5	480	258	+21 32.2	480	293	+13 45.3	480
224	+29 20.3	480	259	+21 18.7	480	294	+13 32.0	480
225	+29 06.2	480	260	+21 05.2	480	295	+13 18.8	480
226	+28 52.1	480	261	+20 51.8	480	296	+13 05.6	480
227	+28 38.1	480	262	+20 38.3	480	297	+12 52.4	480
228	+28 24.0	480	263	+20 24.9	480	298	+12 39.2	480
229	+28 10.0	480	264	+20 11.4	480	299	+12 26.0	480
230	+27 56.0	480	265	+19 58.0	480	300	+12 12.8	480
231	+27 42.1	480	266	+19 44.6	480	301	+11 59.6	480
232	+27 28.1	480	267	+19 31.2	480	302	+11 46.4	480
233	+27 14.2	480	268	+19 17.8	480	303	+11 33.2	480
234	+27 00.3	480	269	+19 04.4	480	304	+11 20.0	480
235	+26 46.5	480	270	+18 51.0	480	305	+11 06.8	480
236	+26 32.6	480	271	+18 37.7	480	306	+10 53.6	480
237	+26 18.8	480	272	+18 24.3	480	307	+10 40.5	480
238	+26 05.0	480	273	+18 10.9	480	308	+10 27.3	480
239	+25 51.2	480	274	+17 57.6	480	309	+10 14.2	480
240	+25 37.4	480	275	+17 44.3	480	310	+10 01.0	480
241	+25 23.7	480	276	+17 30.9	480	311	+09 47.9	480
242	+25 09.9	480	277	+17 17.6	480	312	+09 34.7	480
243	+24 56.2	480	278	+17 04.3	480	313	+09 21.6	480
244	+24 42.5	480	279	+16 51.0	480	314	+09 08.4	480

Table 3 (cont.)
Pointing Positions (J2000)

Num	*Dec*	*NRA*	*Num*	*Dec*	*NRA*	*Num*	*Dec*	*NRA*
315	+08 55.3	480	329	+05 51.7	480	343	+02 49.0	480
316	+08 42.1	480	330	+05 38.6	480	344	+02 36.0	480
317	+08 29.0	480	331	+05 25.6	480	345	+02 23.0	480
318	+08 15.8	480	332	+05 12.5	480	346	+02 10.0	480
319	+08 02.7	480	333	+04 59.5	480	347	+01 57.0	480
320	+07 49.5	480	334	+04 46.4	480	348	+01 44.0	480
321	+07 36.4	480	335	+04 33.4	480	349	+01 31.0	480
322	+07 23.3	480	336	+04 20.3	480	350	+01 18.0	480
323	+07 10.2	480	337	+04 07.3	480	351	+01 05.0	480
324	+06 57.1	480	338	+03 54.2	480	352	+00 52.0	480
325	+06 44.0	480	339	+03 41.2	480	353	+00 39.0	480
326	+06 30.9	480	340	+03 28.1	480	354	+00 26.0	480
327	+06 17.8	480	341	+03 15.1	480	355	+00 13.0	480
328	+06 04.7	480	342	+03 02.0	480	356	+00 00.0	480

TABLE 4
TESTS FOR CLEAN BIAS AND RESOLUTION EFFECTS USING ARTIFICIAL SOURCES

Artificial Source		Detected in Map Flux Density	
Size (FWHM$''$)	Integrated flux density (mJy)	Peak	Integrated
0.1	2	$1.72 \pm .11$[a]	$1.73 \pm .40$
3	2	$1.24 \pm .14$	$1.51 \pm .41$
5	2	0.72	1.39
	6	2.87	5.13
	18	9.43	17.14
	56	30.05	55.25
6	4	$1.42 \pm .20$	$2.88 \pm .51$
9	4	0.79	3.41
	8	$1.78 \pm .18$	$5.80 \pm .54$
	24	6.28	22.5
	72	19.14	70.4
12	16	$2.44 \pm .22$	$11.82 \pm .80$
18	9	0.52	9.2
	15	1.09	13.7
	32	2.57	28.5
	36	$2.80 \pm .16$	24.9 ± 2.15
	96	8.01	91.2
	300	21.2	284
24	500	19.3	421
30	500	12.3	388
	1000	24.4	771

[a]Values with $\pm$ give rms dispersion of at least five trials with sources in varying locations. All other values are means of from 1–3 measurements.